Title

Screening a Library of FDA-Approved and Bioactive Compounds for Antiviral Activity against SARS-CoV-2

Journal

ACS Infectious Diseases, 7(8)

ISSN

2373-8227

Authors

Biering, Scott B
Van Dis, Erik
Wehri, Eddie
et al.

Publication Date

2021-08-13

DOI

10.1021/acsinfecdis.1c00017

Peer reviewed

ACS Infectious Diseases

pubs.acs.org/journal/aidcbc

Article

Screening a Library of FDA-Approved and Bioactive Compounds for Antiviral Activity against SARS-CoV-2

Scott B. Biering, Erik Van Dis, Eddie Wehri, Livia H. Yamashiro, Xammy Nguyenla, Claire Dugast-Darzacq, Thomas G. W. Graham, Julien R. Stroumza, Guillaume R. Golovkine, Allison W. Roberts, Daniel M. Fines, Jessica N. Spradlin, Carl C. Ward, Teena Bajaj, Dustin Dovala, Ursula Schulze-Gamen, Ruchika Bajaj, Douglas M. Fox, Melanie Ott, Niren Murthy, Daniel K. Nomura, Julia Schaletzky,* and Sarah A. Stanley*

Cite This: https://doi.org/10.1021/acsinfecdis.1c00017

Read Online

ACCESS | Metrics & More | Article Recommendations | Supporting Information

ABSTRACT: Severe acute respiratory syndrome coronavirus 2 (SARS-CoV-2), the causative agent of coronavirus disease 2019 (COVID-19), has emerged as a major global health threat. The COVID-19 pandemic has resulted in over 168 million cases and 3.4 million deaths to date, while the number of cases continues to rise. With limited therapeutic options, the identification of safe and effective therapeutics is urgently needed. The repurposing of known clinical compounds holds the potential for rapid identification of drugs effective against SARS-CoV-2. Here, we utilized a library of FDA-approved and well-studied preclinical and clinical compounds to screen for antivirals against SARS-CoV-2 in human pulmonary epithelial cells. We identified 13 compounds that exhibit potent antiviral activity across multiple orthogonal assays. Hits include known antivirals, compounds with anti-inflammatory activity, and compounds targeting host pathways such as kinases and proteases critical for SARS-CoV-2 replication. We identified seven compounds not previously reported to have activity against SARS-CoV-2, including B02, a human RAD51 inhibitor. We further demonstrated that B02 exhibits synergy with remdesivir, the only antiviral approved by the FDA to treat COVID-19, highlighting the potential for combination therapy. Taken together, our comparative compound screening strategy highlights the potential of drug repurposing screens to identify novel starting points for development of effective antiviral mono- or combination therapies to treat COVID-19.

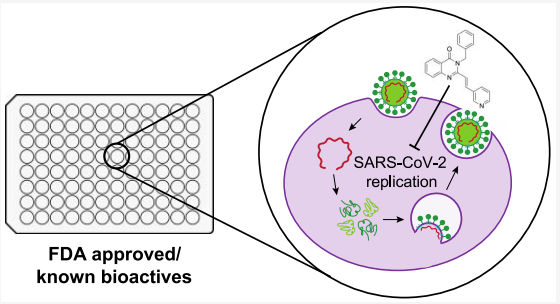

KEYWORDS: *SARS-CoV-2, antiviral, drug repurposing, synergy, B02, remdesivir*

Zoonotic viruses pose a great public health challenge due to the unpredictable nature of an outbreak, the potential to impact an immune-naïve population, and a lack of therapeutic options.[1,2] Coronavirus disease 2019 (COVID-19) is caused by the emergence of the severe acute respiratory syndrome coronavirus 2 (SARS-CoV-2), a member of the *Coronaviridae* family within the *Betacoronavirus* genus.[3−5] The *Betacoronavirus* genus contains several seasonal human pathogens that cause mild disease, as well as the recently emerged severe acute respiratory syndrome coronavirus (SARS-CoV) and Middle East respiratory syndrome coronavirus (MERS-CoV).[4] SARS-CoV-2, SARS-CoV, and MERS-CoV cause severe disease in humans. The increased magnitude of the current pandemic relative to SARS-CoV and MERS-CoV may be explained by increased human−human transmissibility from frequent asymptomatic shedding of this virus.[6−9] Severe cases of COVID-19 are associated with acute respiratory distress syndrome (ARDS) triggered by an inflammatory response resulting in tissue damage and fluid accumulation in the lungs.[10−12] Currently there are limited options to treat patients suffering from severe COVID-19. The sole FDA-approved antiviral compound for COVID-19 treatment is remdesivir; but clinical efficacy is modest, and no conclusive effect on patient mortality has been found.[13−16] Although remdesivir exhibits strong *in vitro* efficacy against SARS-CoV-2 infection, its low exposure in target lung tissue, dose-limiting kidney and liver toxicity, and the need for intravenous administration make early and effective clinical treatment difficult.[17−20] Consequently, the rapid discovery and development of additional therapeutics is vital.

Received: January 12, 2021

Repurposing well-studied preclinical, clinical, and approved compounds holds the greatest potential to swiftly move a drug candidate from the bench to the clinic. An FDA-approved compound library (TargetMol L4200) and a bioactive compound library (TargetMol L4000) are two collections of well-studied compounds, many of which already possess extensive human safety data. Here, we screened both libraries to identify compounds that inhibit SARS-CoV-2 replication in host cells. We report the identification of 13 compounds effective against SARS-CoV-2, 7 of which are previously unreported. Of note, a host-directed compound, the cyclin-dependent kinase (CDK) inhibitor dinaciclib, was determined to be more potent than remdesivir in limiting viral replication in human lung epithelial cells. Additional hit compounds include the following: (i) known antivirals predicted to target SARS-CoV-2 viral factors directly; (ii) host protein kinase and protease inhibitors; and (iii) anti-inflammatory agents. Further, we identify antiviral synergy between remdesivir and the RAD51 inhibitor B02, opening the possibility of clinical combination therapy. Taken together, our results identify several novel starting points for COVID-19 drug development which hold the potential to alleviate the current global pandemic.

RESULTS

Identification of SARS-CoV-2 Permissive Cell Lines for Drug Screening. To design a screen for identification of SARS-CoV-2 antiviral compounds, we first tested a panel of 16 cell lines to identify cells capable of sustaining robust SARS-CoV-2 replication. These cell lines included human pulmonary epithelial and endothelial cells, keratinocytes, hepatocytes, and primate cells, among others (Figure 1 and Figure S1). Multistep growth curves of SARS-CoV-2 in each of these cell lines revealed a range of permissiveness to viral infection (summarized in Table 1). We found distinct cell infection patterns including highly permissive for viral replication (Figure 1A–D) with and without significant cytopathic effect (CPE) (Table 1), mildly permissive with no CPE (Figure S1, Table 1), as well as nonpermissive defined by lack of detectable infectious virus measured by a median tissue culture infectious dose assay (TCID50) (Figure S1, Table 1). We selected the human pulmonary epithelial cell line Calu-3 and the African Green Monkey kidney cell line Vero-E6 for conducting the primary screens, as these cell types supported high levels of infection with dramatic CPE, ideal features for drug screening (Figure 1A,B). We further reasoned that selection of two distinct cell lines would control for cell-specific effects of a given compound.

A Cytopathic Effect-Based Screening Platform to Identify SARS-CoV-2 Antiviral Compounds from the FDA-Approved and Bioactive Compound Libraries. We screened a library of 1,200 FDA-approved compounds (FDA-approved library) and a library of 2,834 preclinical compounds and 1,336 compounds with human clinical data (bioactive library, Figure S2A). For the primary screen, we developed a CPE-based screening assay (CellTiter-Glo, CTG) which uses ATP released from viable cells to drive a luciferase reporter (RLU). This assay identifies drugs that are potent enough to inhibit SARS-CoV-2-mediated cell death, thus selecting for compounds whose antiviral effects are present over several viral lifecycles. Cells are treated with a compound immediately prior to infection with SARS-CoV-2 and incubated until complete CPE is observed in infected vehicle-treated wells, at which time

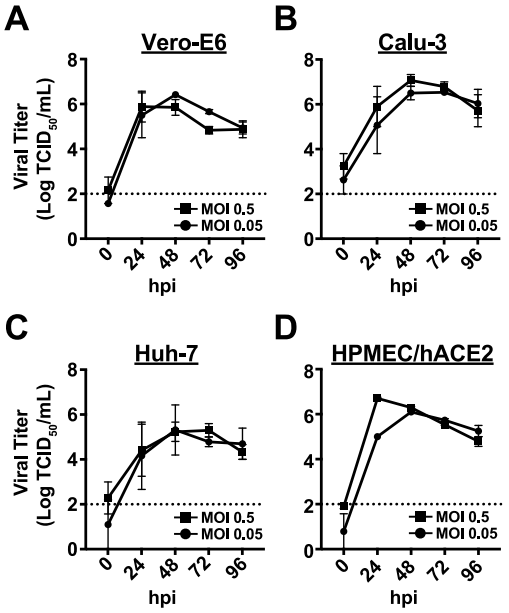

Figure 1. Permissive cell lines to SARS-CoV2 infection. (A) Vero-E6, (B) Calu-3, (C) Huh-7, and (D) HPMEC/hACE2 cells were seeded in 24-well plates and infected with SARS-CoV-2 at MOI 0.5 or 0.05 at 37 °C and 5% CO_2 for 30 min. Viral inoculum was then removed, cells were washed once in 1x PBS, and 1 mL of regular media was replaced. At the indicated time points (hours postinfection, hpi), plates were freeze/thawed, and viral titers from whole cell lysates were analyzed by TCID50 assay. The dashed line represents limit of detection of the assay. Data represent mean ± SEM for n = 2 independent experiments.

cell viability is determined using the CTG assay (Figure 2A). We used both Calu-3 and Vero-E6 cells to identify possible cell type-dependent effects of each compound. We observed significant separation in signal between infected and uninfected wells in Vero-E6 cells at day 3 postinfection (Figure 2B, Z' = 0.47) and in Calu-3 cells at day 4 postinfection (Figure 2C, Z' = 0.43), demonstrating that the assay was suitable for high-throughput screening. Remdesivir served as a positive control in this assay, with EC50 values of 0.7–3 μM (Figure S2B,C). For primary screens, three identical 384-well daughter plates were generated at a final compound concentration of 40 μM. Two plates served as technical replicates that were infected with SARS-CoV-2, while the third functioned as an uninfected cell cytotoxicity control (Figure 2A).

To enable comparative analysis, we ran two parallel screens using the FDA-approved compound library on both Vero-E6 and Calu-3 cells. These screens revealed numerous compounds that significantly inhibited CPE in both cell types without causing significant cytotoxicity in uninfected cells (Figure 2D–F). Intriguingly, although some compounds displayed overlapping antiviral activity in both cell lines, the majority displayed cell specific antiviral activity (Figure 2F). These observations could be explained by species-specific or cell-type-specific mechanisms of action of a given compound or by differences in viral replication between the two cell types. Because we observed cell-type-specific effects of compounds, we proceeded to screen the remaining compounds from the bioactive library using Calu-3 human pulmonary epithelial cells only, which is more physiologically relevant to human infection. Selecting a >1.5 sigma cutoff for the FDA-approved library and a 2.1 cutoff for the bioactive library, our screens

https://doi.org/10.1021/acsinfecdis.1c00017
ACS Infect. Dis. XXXX, XXX, XXX–XXX

Table 1

Cell Line	Species	Origin	Permissive	Cytopathic Effect (CPE)
Vero-E6	African Green Monkey	Kidney Epithelial Cell	yes	+++
Calu-3	Human	Lung Epithelial Cell, adenocarcinoma	yes	+++
HPMEC/hACE2	Human	Lung Microvascular Endothelial Cell, primary	yes	+++
A549/hACE2	Human	Lung Epithelial Cell, carcinoma	yes	++
Huh-7.5.1	Human	Hepatocytes, carcinoma	yes	++
Huh-7	Human	Hepatocytes, carcinoma	yes	+
Caco-2	Human	Colon Epithelial Cell, adenocarcinoma	yes	-
NCI-H1437	Human	Patient Lung Cell derived from metastatic site	yes	-
LNCaP	Human	Prostate Epithelial Cell, carcinoma	yes	-
HaCaT	Human	Keratinocyte, tranformed	yes	-
HCT-116	Human	Colon Epithelial Cell, colorectalcarcinoma	no	-
A549	Human	Lung Epithelial Cell, carcinoma	no	-
HBEC-30KT	Human	Bronchial Epithelial Cell, immortalized	no	-
BEAS-2B	Human	Bronchial Epithelial Cell, transformed	no	-
RD	Human	Derived from the muscle, rhabdomyosarcoma	no	-
HPMEC	Human	Lung Microvascular Endothelial Cell, primary	no	-

identified a total of 140 unconfirmed hits that inhibited SARS-CoV-2-mediated CPE (Figure 2E,F). Best hits were selected for dose−response assays based both on these primary screen data and an assessment of their suitability as potential COVID-19 therapeutics and prioritized for follow-up validation experiments using an experimental pipeline designed to narrow down our list of candidates to only the most promising compounds.

Leveraging the fact that compounds in the FDA-approved and bioactive libraries are well characterized with many drug targets previously defined, we conducted a gene set enrichment analysis (GSEA) of our candidate compounds to shed light on host pathways important for SARS-CoV-2 replication. We found significant enrichment of compounds targeting host cyclin-dependent kinases (CDK1, CDK2, and CDK9), GSK-3β, C-RAF, and JNK1-3, suggesting that ubiquitous host pathways such as cell-cycle progression, MAPK-signaling, as well as GSK-3-signaling are critical for SARS-CoV-2 infection. This agrees with a previously published analysis based on phosphoproteomics of cells infected with SARS-CoV-2[21] (Figure 2G). Thus, our screen suggests these cellular pathways may contain druggable targets for inhibiting SARS-CoV-2 infection of human lung cells.

To validate the *in vitro* potency of drug candidates revealed in our screen, we determined the half-maximal effective concentrations (EC50) of each compound by conducting dose−response curves in the cell line in which compounds were identified using our optimized CTG system as a readout (Figure S2C). Confirmation rates in the secondary dose−response screen were 72% for the Calu-3 and 67% for the Vero-E6 screen, highlighting reproducibility of the assay (Figure 3, Figure S3). Our results identified 17 compounds with EC50 values below 10 μM, including 6 below 5 μM, without significant cytotoxicity. Data for the most potent compounds in Calu-3 cells are shown in Figure 3 and Figure S3. From this list of candidates, the top 12 compounds were selected for downstream validation (Figure 3). Hits were classified into four distinct categories based upon their proposed mechanism of action, including (1) protein kinase and protease inhibitors, (2) anti-inflammatory compounds, (3) direct-acting antivirals, and (4) other host factor-targeting compounds. This set of hits contained compounds with previously reported SARS-CoV-2 antiviral activity (dinaciclib, GC376 sodium, cyclosporin A, and camostat mesylate) and seven compounds that have not previously been reported to have anti-SARS-CoV-2 activity (Table 2).[21−24] Previously unreported compounds include the CDK inhibitor AZD5438, the AKT inhibitor SC66, the VEGFR inhibitor BFH772, the NADPH oxidase inhibitor GKT137831, the RAD51 inhibitor B02, the steroid budesonide, and the anti-inflammatory compound cantharidin.

Confirmation and Characterization of SARS-CoV-2 Antiviral Candidate Compounds. As our CPE-based screening assay measures SARS-CoV-2-induced cell death indirectly through quantification of ATP from viable cells, this assay does not directly test for antiviral activity of a given compound. To confirm the SARS-CoV-2 antiviral activity of our top 12 compound candidates, we tested their capacity to antagonize viral infection of Calu-3 cells through TCID50 and qRT-PCR assays. Also included was the PIKfyve kinase inhibitor apilimod mesylate, identified in Riva et al. 2020.[22] We found all tested candidates possessed significant antiviral activity with reductions of infectious virus and genome equivalents ranging from 1 to 4 logs compared to vehicle control-treated cells (Figure 4A−H). Intriguingly, we found that the CDK inhibitor dinaciclib (EC50 0.13 μM) was more potent in our assays than remdesivir (EC50 2.45 μM) in limiting viral titers in Calu-3 cells as measured by TCID50 and qRT-PCR (Table 2).

Since the antiviral activity of compounds *in vitro* may be cell-type-specific, we tested the capacity of a smaller subset of our candidates (dinaciclib, camostat mesylate, BFH772, budesonide, GC376 sodium, apilimod mesylate, GKT137831, B02, and cyclosporin A) to antagonize virus infection across multiple cell types. Compounds were selected based on their lack of cytotoxicity across all cell lines (data not shown). We utilized an immunofluorescence confocal microscopy assay (IFA) to measure the capacity of these nine compounds to inhibit SARS-CoV-2 replication in three diverse cell lines including Huh-7 (human hepatocytes), human pulmonary microvascular endothelial cells stably expressing the SARS-CoV-2 receptor human ACE2 (HPMEC/hACE2),[25] and Vero-E6 cells (Table 1). Cells were treated with a compound immediately prior to infection with SARS-CoV-2 and incubated for 24−48 h. We then stained for the SARS-CoV-2 nucleoprotein (N) and calculated antiviral activity as % decrease in cell infection compared to vehicle-treated infected cells. We found that the antiviral activity of GC376 sodium and

https://doi.org/10.1021/acsinfecdis.1c00017
ACS Infect. Dis. XXXX, XXX, XXX−XXX

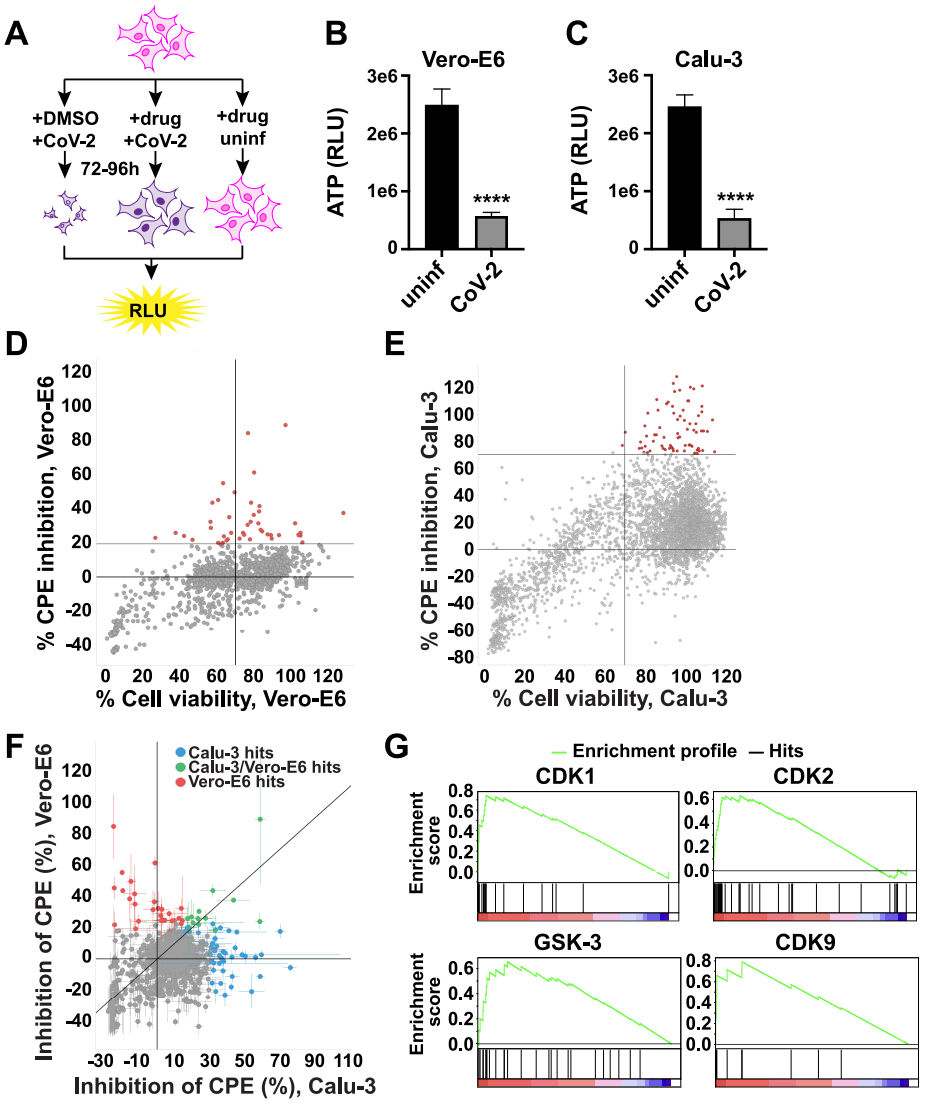

Figure 2. Screening SARS-CoV-2 antiviral activity using the FDA-approved and bioactive compound libraries. (A) Assay scheme: Cells are treated with DMSO (left panel) or drug (middle and right panels), infected with SARS-CoV-2 or left uninfected (right panel), and incubated for 72−96 h to observe cytopathic effect (CPE). CPE is measured by the CTG assay, quantifying ATP content in viable cells using luminescence (RLU). The right panel shows the cytotoxicity control, treating cells with drugs but without virus. (B,C) Average luminescence is shown for (B) Vero-E6 at 72 h or (C) Calu-3 cells at 96 h postinfection. (D) Screen of FDA-approved and bioactive compound libraries on Vero-E6 cells with inhibition of CPE (%) on the *y*-axis and cell viability (%) on the *x*-axis normalized to DMSO-treated wells. Red: high priority hits with a cutoff of >20% inhibition of CPE and >70% cell viability. (E) As in (D), but on Calu-3 cells, with a cutoff of >70% inhibition of CPE and >70% cell viability. (F) Combination of inhibition of CPE (%) on Vero-E6 (*y*-axis) from (D) and Calu-3 (*x*-axis) from (E). (G) Gene set enrichment analysis. Distribution of the enrichment score (green line) across compounds annotated to molecular targets (vertical black lines). CDK1, CDK2, GSK-3 $p < 0.001$, CDK9 $p = 0.0015$. False discovery rate (FDR) $q < 0.05$. Data represent mean ± SEM for $n = 24$ technical replicates (B, C) or $n = 2$ technical replicates (F). ****: $p < 0.0001$.

apilimod mesylate was conserved across these cell lines (Figure 5A,B), while all other tested drugs exhibited cell-type-specific activity (Figure 5C−I). GC376 sodium has been suggested to inhibit SARS-CoV-2 M protease (Mpro),[26] which may explain its efficacy across cell lines.

To shed light on mechanisms of action, we tested whether our top compounds inhibit SARS-CoV-2 Mpro or papain-like protease (PLpro). Conducting in-house developed SARS-CoV-2 protease cleavage assays, we identified disulfiram as a potent PLpro inhibitor and both disulfiram and GC376 sodium as Mpro inhibitors, confirming previous observations[26−28] (Figure S4). Notably, high concentrations of disulfiram exhibited antiviral activity in Calu-3 cells with 3 log reductions of viral titer and genome equivalents in TCID50 and qRT-PCR assays compared to vehicle control-treated cells, potentially explaining its antiviral mechanism of action (Table 2). Although our data indicate that disulfiram is sufficient to inhibit protease activity in an *in vitro* protease assay, its antiviral activity in cell culture may be multifactorial since recent reports have implicated this compound as targeting other SARS-CoV-2 proteins such as nsp13 and nsp14 and is even an inhibitor of pyroptosis via inhibition of gasdermin D.[29,30] Given that disulfiram has been reported to inhibit the function of diverse targets, it may act nonspecifically as a promiscuous inhibitor of SARS-CoV-2 proteins. It is also noteworthy that disulfiram has been reported to lose activity in the presence of reducing agents, and as our protease assays were not conducted in the presence of reducing agents, this

https://doi.org/10.1021/acsinfecdis.1c00017
ACS Infect. Dis. XXXX, XXX, XXX−XXX

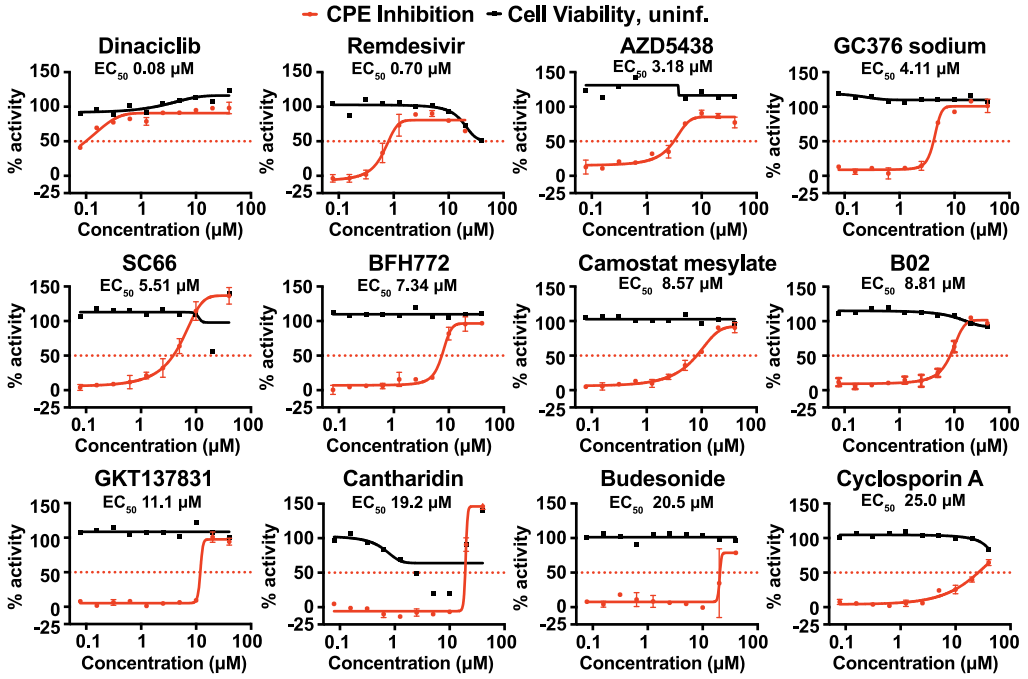

Figure 3. Dose−response curves of compounds with SARS-CoV-2 antiviral activity. Calu-3 cells were infected with SARS-CoV-2 at MOI 0.05 and treated with compounds at indicated concentrations. Data show % CPE inhibition in SARS-CoV-2 infected cells (red) and % cell viability in uninfected cells (black). Data are normalized to the mean of DMSO-treated wells and represent mean ± SD for n = 2 technical replicates.

Table 2

Library	Compound	EC50 (μM)						Category	Previous reports	Clinical trial
		CellTiter Glo	TCID50	qRT-PCR	IFA					
		Calu-3	Calu-3	Calu-3	Vero-E6	HPMEC/hACE	Huh-7			
Bioactive	Dinaciclib	0.08	0.13	0.08	>10	>10	0.04	CDK inhibitor	Bouhaddou et al., Cell 2020, Ellinger et al., Research Square 2020, Wells et al., Nature Communications 2020	
FDA-Approved	Remdesivir	0.70	2.45	1.61	12.30	0.21	> 40	RDRP inhibitor	Jeon et al., BioRxiv 2020, Touret et al., BioRxiv 2020, Riva et al., Nature 2020	yes
FDA-Approved	Camostat mesylate	8.57	0.17	0.56	>40	>40	>40	TMPRSS2 inhibitor	Gordon et al., Nature 2020, Jeon et al., BioRxiv 2020, Vuong et al., Nature Communications 2020	yes
Bioactive	AZD5438	3.18	4.62	2.41	5.25	10.28	N.D.	CDK inhibitor	New	
Bioactive	GC376 sodium	4.11	10.16	5.22	1.61	<1.25	<1.25	3CLpro inhibitor	Ma et al., Cell Research 2020, Iketani et al., BioRxiv 2020	
Bioactive	Cantharidin	19.20	4.84	1.05	>40	N.D.	N.D.	Anti-inflammatory	New	
Bioactive	BFH772	7.34	5.78	24.92	19.45	5.80	4.80	VEGFR kinase inhibitor	New	
Bioactive	SC66	5.51	24.84	8.98	N.D.	N.D.	N.D.	AKT Inhibitor	New	
Bioactive	B02	8.81	20.35	18.24	>40	>40	>40	RAD51 inhibitor	New	
Bioactive	GKT137831	11.10	>40	10.13	>40	17.02	>40	NADPH oxidase inhibitor	New	
Bioactive	Apilimod mesylate	N.D.	21.94	19.00	19.58	<1.25	<1.25	Lipid kinase inhibitor	Bakowski et al., BioRxiv 2020, Dittmar et al., BioRxiv 2020, Riva et al., Nature 2020	yes
FDA-Approved	Disulfiram	>40	15.17	13.16	N.D.	11.72	>40	3CLpro inhibitor	Dittmar et al., BioRx 2020	yes
FDA-Approved	Budesonide	20.50	14.72	>40	>40	16.27	>40	Steroid	New	yes
FDA-Approved	Cyclosporin A	>40	7.54	36.72	14.41	>40	2.78	Calcineurin inhibitor	Dittmar et al., BioRxiv 2020, Jeon et al., BioRxiv 2020	yes

presents a potential confounding factor for clinical translation.[28,31] In summary, these data highlight the benefit of a target-agnostic approach to expose previously unknown mechanisms of identified antivirals, as well as the importance of testing and validation across multiple cell lines for antiviral screening.

Candidate Compound B02 Exhibits Antiviral Synergy with the Nucleoside Analog Remdesivir. Combination therapy is a highly desirable approach for treating SARS-CoV-2 infections.[32] Because our screen revealed only a single compound (dinaciclib) possessing greater antiviral activity than remdesivir when used as a monotherapy, we asked if our compound candidates possess synergistic antiviral activity when used in combination with remdesivir. To assess this, we conducted a CPE inhibition assay using 10 μM of compound in the presence or absence of an EC15 of remdesivir (2 μM, Figure S2B,C) in Vero-E6 cells. Interestingly, the RAD51 inhibitor B02 exhibited potent synergistic activity with remdesivir (Figure 6A). We confirmed these results in Calu-3 cells by conducting a dose−response of remdesivir in the presence or absence of 10 μM B02 and observed a >10-fold shift in the EC50 of remdesivir from 1 μM to <0.08 μM (Figure 6B). To confirm antiviral synergy between B02 and remdesivir, we conducted a checkerboard dose−response matrix of both remdesivir and B02 at doses ranging between 0.1 and 20 μM of B02 and from 0.1 to 10 μM of remdesivir and found significant antiviral synergy across this matrix (Figure 6C,D). We quantified synergy potency by using a computational zero interaction potency (ZIP) modeling system which defines compound synergy as a value >10, a value <10 as additive compound effects, and a value <0 as antagonistic effects.[33] We determined our maximum synergy

https://doi.org/10.1021/acsinfecdis.1c00017
ACS Infect. Dis. XXXX, XXX, XXX−XXX

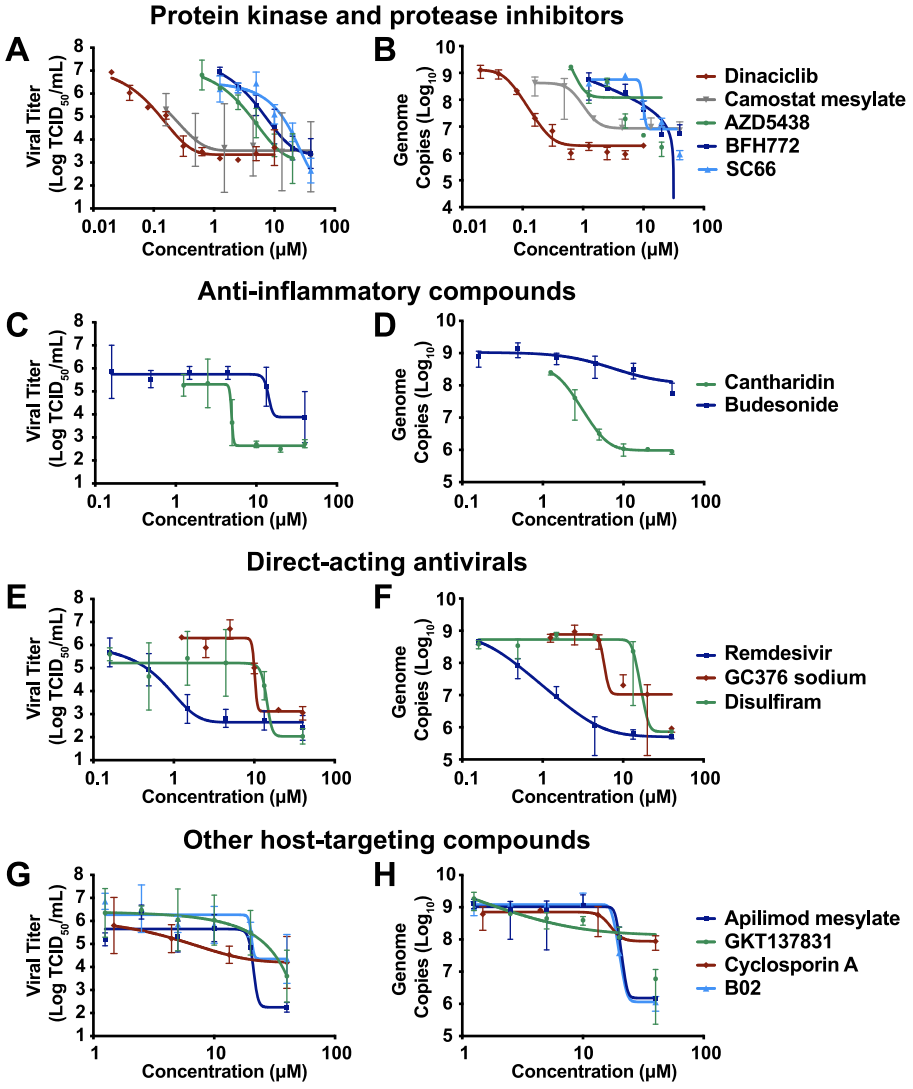

Figure 4. Confirmation and characterization of SARS-CoV-2 antiviral candidate compounds. Calu-3 cells were infected with SARS-CoV-2 at MOI 0.05 and treated with the top 12 compounds (shown in Figure 3), disulfiram, or apilimod mesylate at indicated concentrations, and supernatants were collected at 24 hpi. Viral titers and genome copies were calculated by TCID50 and qRT-PCR, respectively. (A) and (B) protein kinase and protease inhibitors, (C) and (D) anti-inflammatory compounds, (E) and (F) direct-acting antivirals, and (G) and (H) other host-targeting compounds. TCID50 data represent mean ± SD for $n = 2$ independent experiments. Genome copy data represent mean ± SEM for $n = 2$ technical replicates and are representative of $n = 2$ independent experiments.

score to be 22.02, demonstrating antiviral synergy between remdesivir and B02. Taken together, the observation that B02 synergizes with remdesivir provides insight into how antiviral synergy with remdesivir can be achieved, holding the potential for future clinical translation.

DISCUSSION

In this study, we screened a library of FDA-approved, clinical and preclinical compounds for antiviral activity against SARS-CoV-2, with the goal of rapidly repurposing drug candidates for clinical use during the COVID-19 pandemic. We identified multiple cell lines that were permissive to SARS-CoV-2 infection and conducted primary screens using virus-induced CPE as a functional readout in two highly permissive but divergent cell types (Vero-E6 and Calu-3). We identified many compounds displaying varying degrees of antiviral activity across distinct cell lines including Vero-E6, Calu-3, HPMEC/hACE2, and Huh-7. These cell type-dependent phenotypes suggest significant cell type dependency of compound efficacy *in vitro*. We further validated a subset of candidates to define EC50 values, confirmed antiviral activity in orthogonal assays, probed mechanism of action, and demonstrated antiviral synergy of one compound with remdesivir. While our investigation successfully identified compounds published previously, we also identified seven potent compounds that, to our knowledge, have not been previously reported. They include the RAD51 inhibitor B02, the CDK inhibitor AZD5438, the AKT inhibitor SC66, the VEGFR inhibitor BFH772, the NADPH oxidase inhibitor GKT137831, the steroid budesonide, and the anti-inflammatory compound cantharidin. Further, B02 was found to synergize with remdesivir, shifting the apparent EC50 of remdesivir more than 10-fold. This finding presents new insights into mechanisms of antiviral synergy with remdesivir that can be applied toward development of new compounds to be used for remdesivir combination therapy.

The cell type-dependent antiviral efficacy of many of our drug candidates within this screen indicates a strong selection

https://doi.org/10.1021/acsinfecdis.1c00017
ACS Infect. Dis. XXXX, XXX, XXX−XXX

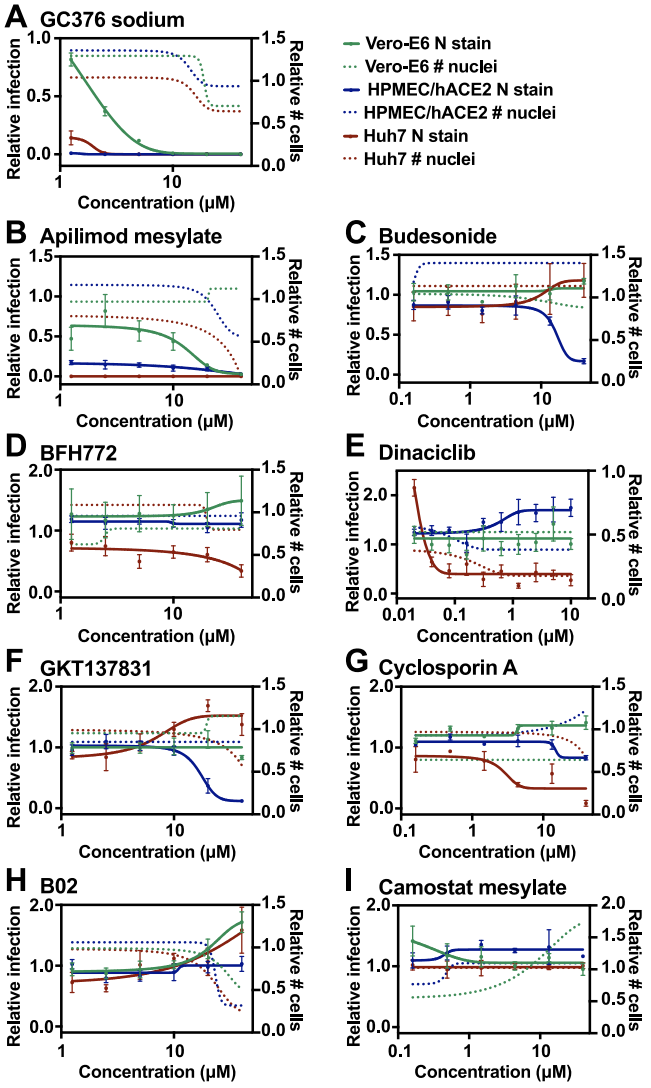

Figure 5. Cell-type-specificity of compounds antiviral activity. Huh-7, HPMEC/hACE2, and Vero-E6 cells were infected with SARS-CoV-2 at MOI 0.05 and treated with (A) GC376 sodium, (B) apilimod mesylate, (C) budesonide, (D) BFH772, (E) dinaciclib, (F) GKT137831, (G) cyclosporin A, (H) B02, and (I) camostat mesylate at indicated concentrations. At 48 hpi, cells were washed, fixed, and stained for SARS-CoV-2 nucleocapsid protein. Plates were fluorescently imaged and analyzed for nucleocapsid stain per nuclei. Relative infection (solid lines) and relative number of cells (dashed lines) are normalized to DMSO-treated wells. Data represent mean ± SEM for $n = 4$ technical replicates and are representative of $n = 3$ independent experiments.

bias is introduced by the selection of cell type used in a screen. The biological reason for this is likely due to distinct cell type-expression patterns of host factors essential for SARS-CoV-2 replication or differential drug metabolism. For example, SARS-CoV-2 requires proteolytic cleavage of the spike (S) glycoprotein by a host protease once it binds to the ACE2 receptor.[34−36] This cleavage can be performed by multiple host proteases including TMPRSS2 and cathepsin L, whose expression levels vary significantly between different cell lines.[34,37,38] Vero-E6 cells do not express TMPRSS2, meaning any drug targeting TMPRSS2, or the interaction between S and TMPRSS2, would not emerge as a hit in such a cell line.[36] Indeed, the drug candidate camostat mesylate, a TMPRSS2 inhibitor currently in clinical trials,[24] inhibited SARS-CoV-2 in Calu-3 but not in Vero-E6 cells (Figure 5). Conversely, GC376 sodium, a previously characterized SARS-CoV-2 protease inhibitor, maintains its antiviral activity across multiple cell lines in our study, suggesting that compounds targeting viral factors may be expected to show activity across different tissues, although the extent of activity can differ based on prodrug metabolism, as previously observed with remdesivir.[26,27,39] Pharmacokinetics and dynamics must be taken into account for each compound and may be influenced by the metabolic state of distinct cell lines or tissue within infected humans. Our comparative cell line investigation of antiviral compounds highlights cell line selection as a critical step when conducting SARS-CoV-2 drug screens and may explain disparate data obtained in different studies.[21,22,40−45] Finally, compound solubility is a confounding factor that must be considered when interpreting data from high-throughput compound screens. Although we visually examined all conditions in our screen during validation experiments, the observed dose−response pattern for cantharidin is consistent with issues of compound solubility (Figure 3).

Defining the mechanisms of action of antiviral compounds is critical to determine how a compound may be modified to improve antiviral efficacy and to suggest the compounds' pharmacokinetic and pharmacodynamic limitations. An advantage of screening libraries of well characterized compounds is that the molecular targets of many compounds are already determined. GSEA analysis of our top antiviral candidates revealed a set of enriched host and viral targets. Our candidate compounds possess distinct mechanisms of action including host kinase and protease inhibition, anti-inflammatory activity, and direct antiviral efficacy targeting virus factors. Our results also implicate host pathways that are critical for SARS-CoV-2 viral replication including regulation of the cell cycle through modulating CDKs, regulating MAPK signaling through modulation of c-JUN N-terminal kinases (JNK), and modulation of glycogen synthase kinase 3 (GSK-3). Our screening results are consistent with other reports that these diverse cellular pathways are likely to be critical for the SARS-CoV-2 lifecycle.[21,46−50] These observations call for further mechanistic investigation of the dependency of SARS-CoV-2 on these various host pathways and highlight the potential of repurposing other drugs not studied here that target these pathways.

Though our study identified many distinct antiviral candidates, only dinaciclib exceeded the *in vitro* potency of remdesivir in our CPE-based screening assay. Therefore, combination therapy may be the best strategy to achieve high efficacy rapidly.[32] Here, we identify the RAD51 inhibitor B02 as synergistic with remdesivir. The mechanism of action of this antiviral synergy is currently unknown and an active area of investigation. While RAD51 is an annotated target of B02, it is unclear if RAD51 inhibition is responsible for the antiviral activity of B02 against SARS-CoV-2. Further, as RAD51 expression is tightly regulated in human cells, the levels of RAD51 in human lung cancer cell lines like Calu-3 may not represent physiological levels present in cells infected by SARS-CoV-2 in patients. In addition, the reported IC50 of B02 for inhibition of RAD51 activity *in vitro* is reported to be 27.4 μM, while we calculated the EC50 of B02 for inhibition of SARS-CoV-2 infection to be 8.81 μM.[51] This discrepancy may be explained by the difference in assays used to assess B02 activity, a difference in function of RAD51 for mediating strand

https://doi.org/10.1021/acsinfecdis.1c00017
ACS Infect. Dis. XXXX, XXX, XXX−XXX

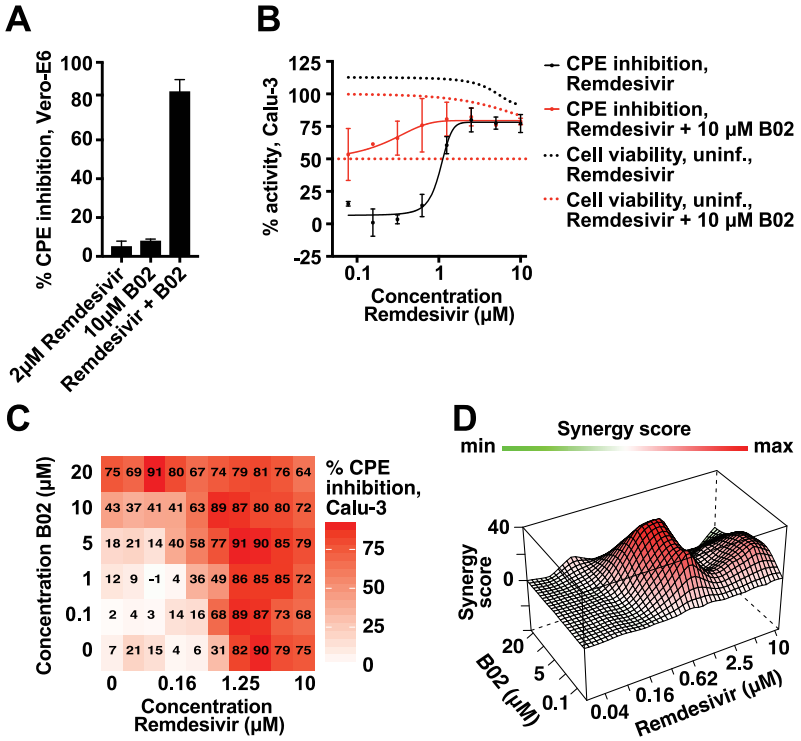

Figure 6. B02 synergy with remdesivir. (A) Vero-E6 cells were infected with SARS-CoV-2 at MOI 0.05 and treated with 2 μM remdesivir, 10 μM B02, or a combination of 2 μM remdesivir and 10 μM B02 for 72 h. CPE inhibition was measured by CTG assay and was normalized to DMSO-treated wells. (B) Calu-3 cells were infected with SARS-CoV-2 at MOI 0.05 and treated with remdesivir at indicated concentrations in the presence or absence of 10 μM B02 for 96 h. Data show % CPE inhibition in SARS-CoV-2 infected cells (solid lines) and % cell viability in uninfected cells (dashed lines) normalized to DMSO-treated wells. (C) Calu-3 cells were infected with SARS-CoV-2 at MOI 0.05 and treated with a dose−response interaction matrix of remdesivir (0 to 10 μM) and B02 (0 to 20 μM). Color gradient indicates % inhibition of CPE normalized to DMSO-treated wells. (D) Three-dimensional surface plot representing synergy score (z-axis) of dose−response interaction matrix between remdesivir and B02 shown in (C). Data represent mean ± SD (A and B) and mean (C) for n = 2 technical replicates.

exchange of nucleic acid vs promoting SARS-CoV-2 replication, or that RAD51 is not the molecular target of B02 required for antiviral activity against SARS-CoV-2 infection. Although, as RAD51 has been previously reported to function in a pro-viral manner as a component of the hepatitis C virus (HCV) membranous replication complex, it is tempting to speculate that RAD51 may comparably promote SARS-CoV-2 replication as a component of its replication complex.[52] If true, the synergy observed between B02 and remdesivir may be due to the simultaneous inhibition of two components of the SARS-CoV-2 replication complex, namely the SARS-CoV-2 RNA-dependent RNA Polymerase (RdRP) by remdesivir[53,54] and of RAD51 by B02. This is further supported by the observation that B02 possesses antiviral activity in the absence of remdesivir suggesting the target of B02 plays a direct role in promoting viral replication. We have previously observed antiviral synergy against SARS-CoV-2 for compounds that possess no antiviral activity on their own against SARS-CoV-2, such as the HCV NS5A inhibitor velpatasvir.[32] This suggests antiviral synergy may arise through direct inhibition of one or more viral factors as well as through modulation of host pathways. Further, as remdesivir is a direct inhibitor of the RdRP, the virus can be thought of as in a "weakened" or "sensitized" state in the presence of remdesivir, potentially making it more vulnerable to additional chemical compounds with no appreciable activity on their own. It should be noted that the pharmacokinetics of B02 makes it unclear if it will be effective in the clinic. Nevertheless, the *in vitro* antiviral synergy we observe between remdesivir and B02 provides a molecular basis for understanding how to achieve remdesivir synergy. Taken together, the potential of combinatorial approaches, ideally against distinct molecular targets, holds promise and should be prioritized for *in vivo* studies to determine efficacy.

At the beginning of the COVID-19 pandemic, many groups utilized a variety of genetic, proteomic, and chemical screening strategies to identify potential drugs for repurposing against SARS-CoV-2. These studies differ in the cell type selected for screening and in the assays used to determine viral replication. Most SARS-CoV-2 drug screens to date have utilized either an IFA-based approach or a CPE-based approach. In general, the IFA-based screens investigate antiviral activity earlier than CPE-based studies (typically 1−2 dpi vs 3−4 dpi, respectively) adding a selection bias for compounds that are effective at early time points, as many compounds with mild antiviral activity (or shorter half-lives) may be overcome by viral replication at later time points. In addition to the need to interpret *in vitro* assay data carefully, our study highlights the importance of cell type selection when screening for antiviral compounds *in vitro*. Use of multiple cell lines is critical. In particular, many early studies used Vero-E6 cells due to their widespread availability, permissiveness to SARS-CoV-2 infection, and ease of use and manipulation. However, we found that activity of compounds against SARS-CoV-2 in Vero-E6 cells does not correlate well with activity in Calu-3 cells, an arguably more relevant human epithelial cell line. Thus, when interpreting *in vitro* antiviral candidates, both cell type, readout, and relative timing of drug and virus addition need to be carefully considered.

https://doi.org/10.1021/acsinfecdis.1c00017
ACS Infect. Dis. XXXX, XXX, XXX−XXX

Although several COVID-19 vaccines have received Emergency Use Authorization by the FDA, pharmaceutical therapies for COVID-19 patients will continue to be urgently needed. Vaccinating enough of the population to achieve herd immunity will take time, and more importantly, even an optimal vaccine will not eliminate severe COVID-19 due to limitations of vaccine use and efficacy in specific populations such as immunocompromised patients. Our study identified seven compounds not previously demonstrated to have antiviral activity with potential for COVID-19 therapy; one of them was synergistic with the approved COVID-19 therapeutic remdesivir. Intriguingly, budesonide has been already studied in clinical trials for COVID-19 treatment because of its anti-inflammatory properties, and if positive, antiviral efficacy should be considered as an additional pharmacodynamic effect. Investigation into the mechanism of action and *in vivo* efficacy of these compounds is of paramount importance, as is defining the safety profiles of these compounds alone and in combination with remdesivir in humans. Such studies are currently underway in our lab as well as in other laboratories, but further collaboration is needed to expedite this process and provide access to preclinical and clinical testing to alleviate the global COVID-19 pandemic.

METHODS

Cells Lines. Multiple cell lines were acquired in this study to determine permissiveness to SARS-CoV-2 for use in drug screens. Vero-E6 cells were acquired from the American Type Culture Collection (ATCC) and maintained in high glucose DMEM (Gibco, Waltham, MA) supplemented with 10% FBS (R&D Systems, Minneapolis, MN), 1X GlutaMAX (Gibco), and 1X PenStrep (Gibco) [D10 media]. Huh-7 and HPMEC cells were obtained from Dr. Eva Harris (UC Berkeley) and maintained in D10 media or endothelial growth medium 2 (EGM-2) using the EGM-2 bullet kit from Lonza, respectively. LNCaP, HaCaT, Caco-2, Calu-3, HCT-116, and A549 cells were obtained from the UC Berkeley Cell Culture Facility and maintained in D10 media. NCI-H1437 and RD cells were obtained from the Cell and Genome Engineering Core at UCSF via Dr. Olga Gulyaeva (UCSF) and Dr. Michael T. McManus (UCSF) and maintained in D10 media. HBEC-30KT and BEAS-2B cells were obtained from Dr. Neil Tay (UCSF) and Dr. Michael T. McManus (UCSF) via Dr. Patrick Mitchell (UC Berkeley) and Dr. Russell Vance (UC Berkeley) and maintained in defined keratinocyte serum free medium (catalog #10744019, ThermoFisher Scientific) and Advanced RPMI containing 5% FBS, 1% L-glutamine, and 1X PenStrep, respectively. Huh-7.5.1 cells were obtained from Dr. Andreas Puschnik (Chan Zuckerberg Biohub) and maintained in D10 media. All cells were maintained in a CO_2 incubator at 37 °C with 5% CO_2. HPMEC/hACE2 and A549/hACE2 cell lines were produced by transducing parental cells with lentivirus encoding the human ACE2 gene followed by puromycin selection (2 μg/mL) for three passages. The hACE2 encoding plasmid was a gift from Hyeryun Choe (Addgene plasmid # 1786; http://n2t.net/addgene:1786; RRID:Addgene_1786).[55]

SARS-CoV-2 Stock Preparation and Infections. The USA-WA1/2020 strain of SARS-CoV-2 was obtained from BEI Resources. The initial stock from BEI was passed through a 0.45 μM syringe filter, and 5 μL of this filtered stock was inoculated onto ∼80% confluent T175 flasks (Nunc, Roskilde, Denmark) of Vero-E6 cells to produce passage 1 of the virus. CPE was monitored daily, and flasks were frozen down when cells exhibited 50−70% cytopathic effect (CPE) (48−72 hpi). Thawed lysates were then collected, and cell debris was pelleted at 3000 × rpm for 20 min. Clarified viral supernatant was then aliquoted, and infectious virus was quantified via a TCID50 assay. To produce passage 2 SARS-CoV-2 working stocks, 5 μL of the passage 1 stock was inoculated onto ∼80% confluent T175 flasks of Vero-E6 cells as described above. Viral titers produced in Vero-E6 cells ranged from 1×10^6−5×10^6 TCID50 units/mL.

Compound Preparation, Drug Screening, and Synergy Experiments. The compound screening and 384-well infection experiments were conducted as described previously[32] and are described below. The FDA-approved drug library (Targetmol) and the Bioactives Library (Targetmol, Wellesley Hills, MA) containing 1,200 compounds and 4,170 compounds, respectively, were stored in dimethyl sulfoxide (DMSO) at 10 mM in 384-well master plates. Remdesivir (T7766, Targetmol) was also stored at 10 mM in DMSO. For drug screening, 2.5×10^3 Vero-E6 cells (12 μL/well) or 1×10^4 Calu-3 (12 μL/well) were seeded in 384-well white optical-bottom tissue culture-treated plates (Nunc) with a Multidrop Combi liquid handling instrument (Thermo Fisher Scientific, Waltham, MA). Cells were incubated for 24 (Vero-E6) or 48 h (Calu-3) at 37 °C and 5% CO_2 before experiments were conducted. For the primary screen, dose−response experiments, and synergy experiments, compounds were prediluted to 4× final concentration (8× for synergy experiments) in high glucose DMEM. Six μL and 3 μL of media (for primary and synergy experiments, respectively) were transferred from compound dilution plates to cells in 384-well plates using a Cybio Well vario liquid handler (Analytik Jena, Jena, Germany), leading to a final concentration of DMSO at 0.4% (v/v) in the assay plate. Primary screens were conducted at 40 μM compound. For the dose−response experiments, 10-point dose−responses were generated by conducting 2-fold dilutions starting at 40 μM for compound confirmation and 10 μM for remdesivir in synergy plates. For all experiments conducted above, cells were incubated with compounds at 37 °C and 5% CO_2 for 1 h before infection.

For all experiments above, cells were infected in 384-well plates at a multiplicity of infection (MOI) of 0.05 in a total volume of 6 μL/well. Cells were harvested for CTG-analysis once complete CPE was observed in DMSO-treated infected wells (72 hpi for Vero-E6 and 96 hpi for Calu-3). For harvest, opaque stickers (Nunc) were applied to the bottoms of plates to minimize signal spillover between wells, and plates were developed with the CellTiter-Glo 2.0 reagent (Promega, Madison, WI) according to the manufacturer's instructions, with the exception of Vero-E6 cells, for which CTG reagent was diluted 1:1 (v/v) in PBS (Gibco, Waltham, MA, USA). Luminescence was read on a Spectramax L (Molecular Devices, San Jose, CA). Each plate contained 24 wells of uninfected/DMSO-treated cells (100% CPE inhibition) and 24 wells infected/DMSO-treated cells (0% CPE inhibition). Average values from those wells were used for data normalization and to determine % CPE inhibition for test compound wells. Duplicate plates were used to calculate average values and standard deviations. Z' was determined as described previously.[56] Statistical significance between experimental conditions was assessed using a two-tailed, heteroscedastic Student's t test. Measurements were taken from distinct samples unless indicated otherwise. The data was plotted and analyzed with Spotfire (Tibco) and GraphPad

https://doi.org/10.1021/acsinfecdis.1c00017
ACS Infect. Dis. XXXX, XXX, XXX−XXX

Prism (San Diego, CA). Synergy scores were quantified using a zero-interaction potency (ZIP) model in SynergyFinder.[33]

GSEA Analysis. The methods for GSEA analysis conducted for this study were previously reported and described below.[32] In brief, candidate compounds identified in our screens were assigned distinct properties based on known host targets and pathways using the Center for Emerging and Neglected Diseases' database and for pharmacokinetic data and transporter inhibition data, the DrugBank database. Each assigned property was tested for enrichment among the screening hits using the gene set enrichment analysis (GSEA) software as described.[22,57,58] Compounds annotated for each property were considered as part of the "gene set". For each set of annotations, the background compound set was defined as the set of compounds annotated for any property. GSEA preranked analysis was performed using the compounds' % CPE inhibition from each screen. Compound sets included in the analysis were between 5 and 500 compounds. The enrichment score (ES) reflects the degree to which a gene set is overrepresented at the top of a ranked list of compounds interacting with the given target. GSEA calculates the ES by walking down the ranked list of compounds interacting with the given target, increasing a running-sum statistic when a gene is in the gene set and decreasing it when it is not.

Immunofluorescence Microscopy Analysis (IFA). One $\times 10^4$ Vero-E6, HPMEC/hACE2, or Huh-7 cells were seeded in black 96-well plates with clear bottoms 24 h before adding drug combinations and infecting with SARS-CoV-2 at MOI 0.05 (viral inoculums were not washed away). Plates were fixed in 4% paraformaldehyde (PFA) 24 hpi (Vero-E6 and HPMEC/hACE2) and 48 hpi (Huh-7), permeabilized using 0.2% saponin in blocking buffer (2% BSA, 1% FBS in PBS) at room temperature for 30 min, incubated with mouse anti-SARS-CoV-2 nucleocapsid protein (1:1000, Sino Biological, Beijing, China; 40145-MM05) overnight in blocking buffer, incubated with goat antimouse AlexaFluor647 (1:1000, Abcam, Cambridge, United Kingdom) and DAPI/Hoechst (1:1000, Invitrogen) in blocking buffer, fixed in 4% PFA, and kept in 1x PBS until imaging on an Image Xpress Micro 4 (Molecular Devices). An average of 1×10^3 cells was imaged across four sites per well and analyzed for nucleocapsid (N) stain per nuclei (DAPI) using CellProfiler 3.1.9 (Broad Institute, Cambridge, MA).

TCID50 Assay. Five $\times 10^4$ Calu-3 cells were seeded into 96-well plates 48 h before adding drug combinations and viral inoculum (MOI 0.05) (viral inoculum was not washed away). At 24 hpi, the supernatant was collected from each well and serially diluted, and each dilution was applied to eight wells in 96-well plates containing Vero-E6 cells. Three days later, CPE was counted visually, and TCID50/mL was calculated using the dilution factor required to produce CPE in half, or 4/8, of the wells for a given dilution.

RT-qPCR. RT-qPCR was conducted as previously reported[32] and further described below. For RT-qPCR, supernatants were collected at 48 hpi and inactivated 1:1 in 1X DNA/RNA Shield for RNA extraction and RT-qPCR analysis (Zymo Research, Irvine, CA). RNA was extracted using the QIAamp Viral RNA Mini Kit (Qiagen, Hilden, Germany) according to the manufacturer's instructions. In brief, 140 μL of each sample was mixed with 560 μL of Carrier-RNA-containing AVL and incubated for 10 min at RT. After addition of 560 μL of 100% ethanol, the samples were spun through columns. The columns were washed sequentially with 500 μL of AW1 and 500 μL AW2, and RNA was eluted using 50 μL of RNase free water. RT-qPCR reactions with TaqPath master mix (Thermo Fisher) were assembled following the manufacturer's instructions. For a 20 μL reaction, 5 μL of 4x TaqPath master mix was combined with 1.5 μL of SARS-CoV-2 (2019-nCoV) CDC N1, N2, or RNase P qPCR Probe mixture (Integrated DNA Technologies, Cat. #10006606, Primer sequences: 2019-nCoV_N1-F 2019-nCoV_N1: GAC CCC AAA ATC AGC GAA AT; 2019-nCoV_N1-R 2019-nCoV_N1: TCT GGT TAC TGC CAG TTG AAT CTG; 2019-nCoV_N1−P 2019-nCoV_N1 FAM: ACC CCG CAT TAC GTT TGG TGG ACC-BHQ1), RNA sample, and water to a final volume of 20 μL. Volumes were divided by 2 for 10 μL reactions. RT-qPCR was performed on a BioRad CFX96 or CFX384 instrument with the following cycle: 1) 25 °C for 1 min, 2) 50 °C for 15 min, 3) 95 °C for 2 min, 4) 95 °C for 3 s, 5) 55 °C for 30 s (read fluorescence), 6) go to step 4 for 44 repetitions. Quantification cycle (Cq) values were determined using the second derivative peak method.[59] Custom code written in MATLAB (available at https://gitlab.com/tjian-darzacq-lab/second-derivative-cq-analysis) was used to take the numerical second derivative of fluorescence intensity with respect to cycle number, using a sliding window of ±3 cycles. The peak of the second derivative was fit to a parabola, whose center was taken to be the Cq value.[59]

SARS-CoV-2 MPro Activity Assay. Compounds were dissolved in DMSO at 50X the desired screening concentration. DMSO was used as a solvent control. MPro protein (purification described below) was diluted in assay buffer (50 mM HEPES pH 7.5, 150 mM NaCl, 1 mM EDTA, 0.01% pluronic acid F127) to a concentration of 30 nM, and 24.5 μL of diluted protein was aliquoted to each well of a black 384-well plate (Corning 384-Well, Flat-Bottom Microplate). Each well was treated with 0.5 μL of compound or vehicle, and the plate was incubated for 30 min at room temperature. During the compound incubation, the peptide probe KTSAVLQ-Rh110-gammaGlu (Biosyntan) was diluted from 5 mM DMSO stock into assay buffer. After preincubation, 5 μL of 75 μM Rh-110 probe was added to each well. The RFU value was immediately measured on a Tecan Spark plate reader with an excitation wavelength of 488 nm and an emission wavelength of 535 nm at 30 °C for 30 min.

Purification of SARS-CoV-2 Main Protease. The coding sequence for SARS-CoV-2 main protease was codon-optimized for *E. coli* and synthesized by Integrated DNA Technologies. The sequence was amplified by PCR and cloned into the pGEX6P-1 vector, downstream of GST and an HRV 3C protease cleavage site, using the Gibson Assembly Master Mix kit (New England BioLabs, Inc.). To ensure authentic termini, the amino acids AVLQ were added to the N-terminus of the main protease by addition of their coding sequence to the 5′ end of the gene product. This sequence reconstitutes the SARS-CoV-2 NSP4/5 cleavage site, resulting in autocleavage by the main protease protein product.[60] Similarly, we added a GP-6xHis tag for IMAC purification to the C-terminus (the GP completes a nonconsensus 3C cleavage site along with the C-terminus of the main protease which allows for cleavage of the His tag after purification, resulting in an authentic C-terminus).

HI-Control BL21(DE3) cells were transformed with the expression plasmid using standard techniques. We used HI-Control cells, as we observed expression of the main protease was toxic in other standard *E. coli* cell lines. A single colony was

https://doi.org/10.1021/acsinfecdis.1c00017
ACS Infect. Dis. XXXX, XXX, XXX−XXX

used to start an overnight culture in LB + carbenicillin media. This culture was used to inoculate 2 × 1 L cultures in Terrific Broth, supplemented with 50 mM sodium phosphate pH 7.0 and 100 μg/mL carbenicillin. These cultures grew in Fernbach flasks at 37 °C while shaking at 225 rpm, until the OD600 reached approximately 2.0, at which point the temperature was reduced to 20 °C, and 0.5 mM IPTG (final) was added to each culture. The cells were allowed to grow overnight.

The next day, the cultures were centrifuged at 6,000*g* for 20 min at 4 °C, and the resulting cell pellets were resuspended in IMAC_A buffer (50 mM Tris pH 8.0, 400 mM NaCl, 1 mM TCEP). Cells were lysed with two passes through a cell homogenizer (Microfluidics model M-110P) at 18,000 psi. The lysate was clarified with centrifugation at 42,000*g* for 30 min, and the cleared lysate was loaded onto 3 × 5 mL HiTrap Ni-NTA columns (GE) pre-equilibrated with IMAC_A buffer, using an AKTA Pure FPLC. After loading, the columns were washed with IMAC_A buffer until the A280 levels reached a sustained baseline. The protein was then eluted with a linear gradient with IMAC_B buffer (50 mM Tris pH 8.0, 400 mM NaCl, 500 mM imidazole, 1 mM TCEP) across 25 column volumes, while 2 mL fractions were collected automatically. Peak fractions were analyzed by SDS-PAGE, and those containing SARS-CoV-2 main protease were pooled. Importantly, autocleavage of the N-terminal GST tag was observed, and the eluted protein had a mass consistent with SARS-CoV-2 main protease along with the C-terminal GP-6xHis tag, as determined by ESI-LC/MS.

Pooled fractions were treated with HRV 3C protease (also known as "PreScission" protease) while dialyzing against IMAC_A buffer at room temperature (2 × 2 L dialyses). Room temperature dialysis was important, as we observed a tendency for the main protease protein to precipitate with prolonged exposure to 4 °C. Cleavage of the C-terminal GP-6xHis tag was confirmed after 2 h by ESI-LC/MS. The dialyzed and cleaved protein was then rerun through a 5 mL HiTrap Ni-NTA column pre-equilibrated with IMAC_A buffer. The main protease eluted in the flow-through as expected.

The protein was then concentrated to approximately 5 mL and loaded onto a Superdex 75 16/60 column pre-equilibrated with SEC Buffer (25 mM HEPES pH 7.5, 150 mM NaCl, 1 mM TCEP). The protein was run through the column at 1 mL/min and eluted as one large peak well in the included volume (at ∼75 mL). Fractions from this peak were analyzed by SDS-PAGE, and pure fractions were pooled and concentrated to 10 mg/mL, aliquoted, and stored at −80 °C. Final yield was typically in the realm of 60−70 mg/L of culture.

SARS-CoV-2 PLpro Activity Assay. Compounds were dissolved in DMSO at 50X the desired screening concentration. DMSO was used as a solvent control. PLpro protein was purified as described below. The screening assay was performed in black 384-well plates (Corning 384-Well, Flat-Bottom Microplate) and in a 25.5 μL volume which contained a final PLpro concentration of 50 nM, a 50 μM concentration of substrate (RLRGG-AMC), and 0.5 μL of DMSO or compound (final concentration of 40 μM); the final assay buffer contained 20 mM Hepes pH 7.5, 100 mM NaCl, and 0.1% mg/mL BSA. Screens were performed with 1:5000 antifoam to reduce the surface tension and bubbles. After addition of the substrate, the RFU value was measured on a Tecan Spark plate reader with an excitation wavelength of 360 nm and an emission wavelength of 460 nm at 30 °C for 30 min.

Expression and Purification of PLpro. The papain-like protease (PLpro) expressing plasmid, 2BT-Nsp3-PLpro, was transformed into *E. coli* BL21 (DE3) and plated on ampicillin resistant LB agar plate. The next day, a colony was picked up for overnight culture in the presence of ampicillin 100 μg/mL. For large-scale protein purification, a 1 L culture of 2XYT media was grown using overnight culture (1:100) at 37 °C (210 rpm). The bacterial culture was grown to an OD600 ∼0.8−1.0 and induced with 1 mM IPTG. The protein was expressed at 20 °C overnight (18−20 h). The bacterial culture was harvested at 4000 × g, and cell pellets were resuspended in 30 mL of lysis buffer (25 mM Tris-HCl pH 8.0, 250 mM NaCl, 10% glycerol, 5 mM β-mercaptoethanol) and supplemented with protease inhibitor tablets. The cell culture was sonicated at 20% amplitude for 7 min (0.5 s ON, 1.5 s OFF). Cellular debris was pelleted down by centrifuging at 15,000 × g for 20 min at 4 °C. The supernatant was loaded on a Talon column (GE Healthcare Life Sciences) (pre-equilibrated with lysis buffer) at a speed of 1 mL/min. Nonspecific proteins were washed with 20 column volumes of Buffer-A (lysis buffer supplemented with 25 mM imidazole). PLpro protein was eluted with 5 column volumes of Buffer-B (lysis buffer supplemented with 250 mM imidazole). The eluted protein was concentrated using a 10 kDa MWCO filter (Amicon-Millipore) and concentrated up to 2 mg/mL.

■ ASSOCIATED CONTENT

Supporting Information

The Supporting Information is available free of charge at https://pubs.acs.org/doi/10.1021/acsinfecdis.1c00017.

Figure S1, related to Figure 1: growth curves of SARS-CoV-2 in various cell lines; Figure S2, related to Figure 2: screening SARS-CoV-2 antiviral activity using FDA-approved and bioactive compound libraries; Figure S3, related to Figure 3: dose−response curves of compounds with SARS-CoV-2 antiviral activity; and Figure S4, related to Figure 4: screening compounds for inhibition of SARS-CoV-2 protease activity (PDF)

■ AUTHOR INFORMATION

Corresponding Authors

Julia Schaletzky − *The Henry Wheeler Center for Emerging and Neglected Diseases, Berkeley, California 94720, United States*; Email: jschaletzky@berkeley.edu

Sarah A. Stanley − *School of Public Health, Division of Infectious Diseases and Vaccinology and Department of Molecular and Cell Biology, Division of Immunology and Pathogenesis, University of California, Berkeley, Berkeley, California 94720, United States*; orcid.org/0000-0002-4182-9048; Email: sastanley@berkeley.edu

Authors

Scott B. Biering − *School of Public Health, Division of Infectious Diseases and Vaccinology, University of California, Berkeley, Berkeley, California 94720, United States*

Erik Van Dis − *Department of Molecular and Cell Biology, Division of Immunology and Pathogenesis, University of California, Berkeley, Berkeley, California 94720, United States*

https://doi.org/10.1021/acsinfecdis.1c00017
ACS Infect. Dis. XXXX, XXX, XXX−XXX

Eddie Wehri − *The Henry Wheeler Center for Emerging and Neglected Diseases, Berkeley, California 94720, United States*
Livia H. Yamashiro − *School of Public Health, Division of Infectious Diseases and Vaccinology and Department of Molecular and Cell Biology, Division of Immunology and Pathogenesis, University of California, Berkeley, Berkeley, California 94720, United States*
Xammy Nguyenla − *School of Public Health, Division of Infectious Diseases and Vaccinology, University of California, Berkeley, Berkeley, California 94720, United States*
Claire Dugast-Darzacq − *Department of Molecular and Cell Biology, Division of Biochemistry, Biophysics and Structural Biology, University of California, Berkeley, Berkeley, California 94720, United States*
Thomas G. W. Graham − *Department of Molecular and Cell Biology, Division of Biochemistry, Biophysics and Structural Biology, University of California, Berkeley, Berkeley, California 94720, United States*
Julien R. Stroumza − *The Henry Wheeler Center for Emerging and Neglected Diseases, Berkeley, California 94720, United States*
Guillaume R. Golovkine − *Department of Molecular and Cell Biology, Division of Immunology and Pathogenesis, University of California, Berkeley, Berkeley, California 94720, United States*
Allison W. Roberts − *Department of Molecular and Cell Biology, Division of Immunology and Pathogenesis, University of California, Berkeley, Berkeley, California 94720, United States*
Daniel M. Fines − *Department of Molecular and Cell Biology, Division of Immunology and Pathogenesis, University of California, Berkeley, Berkeley, California 94720, United States*
Jessica N. Spradlin − *Departments of Chemistry, Molecular and Cell Biology, and Nutritional Sciences and Toxicology, University of California, Berkeley, Berkeley, California 94720, United States*
Carl C. Ward − *Departments of Chemistry, Molecular and Cell Biology, and Nutritional Sciences and Toxicology, University of California, Berkeley, Berkeley, California 94720, United States*
Teena Bajaj − *Department of Bioengineering, University of California, Berkeley, Berkeley, California 94720, United States*
Dustin Dovala − *Novartis Institutes for BioMedical Research, Emeryville, California 94608, United States*
Ursula Schulze-Gamen − *QBI Coronavirus Research Group Structural Biology Consortium, University of California, San Francisco, California 94158, United States*
Ruchika Bajaj − *Department of Bioengineering and Therapeutic Sciences, University of California, San Francisco, San Francisco, California 94158, United States;* orcid.org/0000-0002-9777-0364
Douglas M. Fox − *School of Public Health, Division of Infectious Diseases and Vaccinology and Department of Molecular and Cell Biology, Division of Immunology and Pathogenesis, University of California, Berkeley, Berkeley, California 94720, United States*
Melanie Ott − *Department of Medicine, Medical Scientist Training Program, Biomedical Sciences Graduate Program, University of California, San Francisco, San Francisco, California 94143, United States; J. David Gladstone Institutes, San Francisco, California 94158, United States*
Niren Murthy − *Department of Bioengineering, University of California, Berkeley, Berkeley, California 94720, United States; Innovative Genomics Institute (IGI), Berkeley, California 94704, United States*
Daniel K. Nomura − *Departments of Chemistry, Molecular and Cell Biology, and Nutritional Sciences and Toxicology, University of California, Berkeley, Berkeley, California 94720, United States;* orcid.org/0000-0003-1614-8360

Complete contact information is available at: https://pubs.acs.org/10.1021/acsinfecdis.1c00017

Author Contributions

S.B.B., E.V.D., E.W., L.H.Y, and X.N. contributed equally. Conceptualization: S.B.B., E.V.D., E.W., L.H.Y, X.N., Do.M.F., J.S., S.A.S. Funding acquisition: M.O., N.M., D.K.N., J.S., S.A.S. Investigation: S.B.B., E.V.D., E.W., L.H.Y., X.N., C.D., T.G.W.G., J.R.S., G.R.G., A.W.R., Da.M.F., J.N.S., C.C.W., T.B., D.D., U.S.G., R.B., Do.M.F. Methodology: S.B.B., E.V.D., E.W., L.H.Y., X.N., N.M., D.K.N., J.S., S.A.S. Project administration: J.S., S.A.S. Supervision: M.O., N.M., D.K.N., J.S., S.A.S. Visualization: S.B.B., E.V.D., E.W., L.H.Y., X.N., J.R.S., Do.M.F., J.S., S.A.S. Writing−original draft: S.B.B. Writing−review and editing: S.B.B., E.V.D., E.W., L.H.Y., X.N., Do.M.F., J.S., S.A.S.

Notes

The authors declare no competing financial interest.

■ ACKNOWLEDGMENTS

We thank Dr. Ella Hartenian (UC Berkeley) and Dr. Britt Glaunsinger (UC Berkeley) for assistance with cloning the human ACE2 gene into a lentivirus construct. We thank Dr. Patrick S. Mitchell (UC Berkeley/University of Washington), Dr. Olga Gulyaeva (UCSF), Dr. Andreas Puschnik (Chan Zuckerberg Biohub), and Dr. Eva Harris for cell lines used in this study and helpful discussions. We further thank members of the Harris and Stanley laboratories for helpful discussions. We would like to acknowledge receipt of diverse cell lines used in this study from the UCB Cell Culture facility which is supported by the University of California, Berkeley. SARS-CoV-2 clinical isolate USA-WA1/2020, NR-52281 was obtained through BEI resources, NIAID, NIH and deposited by the Centers of Disease Control and Prevention. This project was supported by generous funding from Eric and Wendy Schmidt by recommendation of the Schmidt Futures program, through Covid Catalyst funding administered by the Center of Emerging and Neglected Diseases at UC Berkeley and through Fast Grants (part of Emergent Ventures at George Mason University). S.B.B. and A.W.R are Open Philanthropy Awardees of the Life Sciences Research Foundation. E.V.D. is supported by NSF Graduate Research Fellowship DGE-1752814. C.D.D. and T.G.W.G. are supported by the Bowes Research Fellows Program N7342, the Siebel Stem Cell Institute W6188, the Jane Coffin Childs Memorial Fund for Medical Research, and the HHMI.

■ REFERENCES

(1) Woolhouse, M., Scott, F., Hudson, Z., Howey, R., and Chase-Topping, M. (2012) Human viruses: discovery and emergence. *Philos. Trans. R. Soc., B 367* (1604), 2864−71.
(2) Lindahl, J. F., and Grace, D. (2015) The consequences of human actions on risks for infectious diseases: a review. *Infect Ecol Epidemiol 5*, 30048.

(3) da Costa, V. G., Moreli, M. L., and Saivish, M. V. (2020) The emergence of SARS, MERS and novel SARS-2 coronaviruses in the 21st century. *Arch. Virol. 165* (7), 1517−1526.
(4) Paules, C. I., Marston, H. D., and Fauci, A. S. (2020) Coronavirus Infections-More Than Just the Common Cold. *JAMA 323* (8), 707−708.
(5) Hartenian, E., Nandakumar, D., Lari, A., Ly, M., Tucker, J. M., and Glaunsinger, B. A. (2020) The molecular virology of coronaviruses. *J. Biol. Chem. 295* (37), 12910−12934.
(6) Gandhi, M., Yokoe, D. S., and Havlir, D. V. (2020) Asymptomatic Transmission, the Achilles' Heel of Current Strategies to Control Covid-19. *N. Engl. J. Med. 382* (22), 2158−2160.
(7) Arons, M. M., Hatfield, K. M., Reddy, S. C., Kimball, A., James, A., Jacobs, J. R., Taylor, J., Spicer, K., Bardossy, A. C., Oakley, L. P., Tanwar, S., Dyal, J. W., Harney, J., Chisty, Z., Bell, J. M., Methner, M., Paul, P., Carlson, C. M., McLaughlin, H. P., Thornburg, N., Tong, S., Tamin, A., Tao, Y., Uehara, A., Harcourt, J., Clark, S., Brostrom-Smith, C., Page, L. C., Kay, M., Lewis, J., Montgomery, P., Stone, N. D., Clark, T. A., Honein, M. A., Duchin, J. S., Jernigan, J. A., and Team, P. H. S. a. K. C. a. C. C.-I. (2020) Presymptomatic SARS-CoV-2 Infections and Transmission in a Skilled Nursing Facility. *N. Engl. J. Med. 382* (22), 2081−2090.
(8) Guan, W. J., Ni, Z. Y., Hu, Y., Liang, W. H., Ou, C. Q., He, J. X., Liu, L., Shan, H., Lei, C. L., Hui, D. S. C., Du, B., Li, L. J., Zeng, G., Yuen, K. Y., Chen, R. C., Tang, C. L., Wang, T., Chen, P. Y., Xiang, J., Li, S. Y., Wang, J. L., Liang, Z. J., Peng, Y. X., Wei, L., Liu, Y., Hu, Y. H., Peng, P., Wang, J. M., Liu, J. Y., Chen, Z., Li, G., Zheng, Z. J., Qiu, S. Q., Luo, J., Ye, C. J., Zhu, S. Y., Zhong, N. S., and Covid-19, C. M. T. E. G. f. (2020) Clinical Characteristics of Coronavirus Disease 2019 in China. *N. Engl. J. Med. 382* (18), 1708−1720.
(9) Rothe, C., Schunk, M., Sothmann, P., Bretzel, G., Froeschl, G., Wallrauch, C., Zimmer, T., Thiel, V., Janke, C., Guggemos, W., Seilmaier, M., Drosten, C., Vollmar, P., Zwirglmaier, K., Zange, S., Wölfel, R., and Hoelscher, M. (2020) Transmission of 2019-nCoV Infection from an Asymptomatic Contact in Germany. *N. Engl. J. Med. 382* (10), 970−971.
(10) Xu, Z., Shi, L., Wang, Y., Zhang, J., Huang, L., Zhang, C., Liu, S., Zhao, P., Liu, H., Zhu, L., Tai, Y., Bai, C., Gao, T., Song, J., Xia, P., Dong, J., Zhao, J., and Wang, F. S. (2020) Pathological findings of COVID-19 associated with acute respiratory distress syndrome. *Lancet Respir. Med. 8* (4), 420−422.
(11) Zhang, B., Zhou, X., Qiu, Y., Song, Y., Feng, F., Feng, J., Song, Q., Jia, Q., and Wang, J. (2020) Clinical characteristics of 82 cases of death from COVID-19. *PLoS One 15* (7), No. e0235458.
(12) Yang, X., Yu, Y., Xu, J., Shu, H., Xia, J., Liu, H., Wu, Y., Zhang, L., Yu, Z., Fang, M., Yu, T., Wang, Y., Pan, S., Zou, X., Yuan, S., and Shang, Y. (2020) Clinical course and outcomes of critically ill patients with SARS-CoV-2 pneumonia in Wuhan, China: a single-centered, retrospective, observational study. *Lancet Respir. Med. 8* (5), 475−481.
(13) Grein, J., Ohmagari, N., Shin, D., Diaz, G., Asperges, E., Castagna, A., Feldt, T., Green, G., Green, M. L., Lescure, F. X., Nicastri, E., Oda, R., Yo, K., Quiros-Roldan, E., Studemeister, A., Redinski, J., Ahmed, S., Bernett, J., Chelliah, D., Chen, D., Chihara, S., Cohen, S. H., Cunningham, J., D'Arminio Monforte, A., Ismail, S., Kato, H., Lapadula, G., L'Her, E., Maeno, T., Majumder, S., Massari, M., Mora-Rillo, M., Mutoh, Y., Nguyen, D., Verweij, E., Zoufaly, A., Osinusi, A. O., DeZure, A., Zhao, Y., Zhong, L., Chokkalingam, A., Elboudwarej, E., Telep, L., Timbs, L., Henne, I., Sellers, S., Cao, H., Tan, S. K., Winterbourne, L., Desai, P., Mera, R., Gaggar, A., Myers, R. P., Brainard, D. M., Childs, R., and Flanigan, T. (2020) Compassionate Use of Remdesivir for Patients with Severe Covid-19. *N. Engl. J. Med. 382* (24), 2327−2336.
(14) Horby, P., Lim, W. S., Emberson, J. R., Mafham, M., Bell, J. L., Linsell, L., Staplin, N., Brightling, C., Ustianowski, A., Elmahi, E., Prudon, B., Green, C., Felton, T., Chadwick, D., Rege, K., Fegan, C., Chappell, L. C., Faust, S. N., Jaki, T., Jeffery, K., Montgomery, A., Rowan, K., Juszczak, E., Baillie, J. K., Haynes, R., Landray, M. J., and Group, R. C. (2021) Dexamethasone in Hospitalized Patients with Covid-19. *N. Engl. J. Med. 384* (8), 693−704.
(15) Beigel, J. H., Tomashek, K. M., Dodd, L. E., Mehta, A. K., Zingman, B. S., Kalil, A. C., Hohmann, E., Chu, H. Y., Luetkemeyer, A., Kline, S., Lopez de Castilla, D., Finberg, R. W., Dierberg, K., Tapson, V., Hsieh, L., Patterson, T. F., Paredes, R., Sweeney, D. A., Short, W. R., Touloumi, G., Lye, D. C., Ohmagari, N., Oh, M. D., Ruiz-Palacios, G. M., Benfield, T., Fätkenheuer, G., Kortepeter, M. G., Atmar, R. L., Creech, C. B., Lundgren, J., Babiker, A. G., Pett, S., Neaton, J. D., Burgess, T. H., Bonnett, T., Green, M., Makowski, M., Osinusi, A., Nayak, S., Lane, H. C., and Members A.-S. G. (2020) Remdesivir for the Treatment of Covid-19 - Final Report. *N. Engl. J. Med. 383* (19), 1813−1826.
(16) Pan, H., Peto, R., Henao-Restrepo, A. M., Preziosi, M. P., Sathiyamoorthy, V., Abdool Karim, Q., Alejandria, M. M., Hernández García, C., Kieny, M. P., Malekzadeh, R., Murthy, S., Reddy, K. S., Roses Periago, M., Abi Hanna, P., Ader, F., Al-Bader, A. M., Alhasawi, A., Allum, E., Alotaibi, A., Alvarez-Moreno, C. A., Appadoo, S., Asiri, A., Aukrust, P., Barratt-Due, A., Bellani, S., Branca, M., Cappel-Porter, H. B. C., Cerrato, N., Chow, T. S., Como, N., Eustace, J., García, P. J., Godbole, S., Gotuzzo, E., Griskevicius, L., Hamra, R., Hassan, M., Hassany, M., Hutton, D., Irmansyah, I., Jancoriene, L., Kirwan, J., Kumar, S., Lennon, P., Lopardo, G., Lydon, P., Magrini, N., Maguire, T., Manevska, S., Manuel, O., McGinty, S., Medina, M. T., Mesa Rubio, M. L., Miranda-Montoya, M. C., Nel, J., Nunes, E. P., Perola, M., Portolés, A., Rasmin, M. R., Raza, A., Rees, H., Reges, P. P. S., Rogers, C. A., Salami, K., Salvadori, M. I., Sinani, N., Sterne, J. A. C., Stevanovikj, M., Tacconelli, E., Tikkinen, K. A. O., Trelle, S., Zaid, H., Røttingen, J. A., Swaminathan, S., and Consortium W. S. T. (2021) Repurposed Antiviral Drugs for Covid-19 - Interim WHO Solidarity Trial Results. *N. Engl. J. Med. 384* (6), 497−511.
(17) Jorgensen, S. C. J., Kebriaei, R., and Dresser, L. D. (2020) Remdesivir: Review of Pharmacology, Pre-clinical Data, and Emerging Clinical Experience for COVID-19. *Pharmacotherapy 40* (7), 659−671.
(18) Goldman, J. D., Lye, D. C. B., Hui, D. S., Marks, K. M., Bruno, R., Montejano, R., Spinner, C. D., Galli, M., Ahn, M. Y., Nahass, R. G., Chen, Y. S., SenGupta, D., Hyland, R. H., Osinusi, A. O., Cao, H., Blair, C., Wei, X., Gaggar, A., Brainard, D. M., Towner, W. J., Muñoz, J., Mullane, K. M., Marty, F. M., Tashima, K. T., Diaz, G., and Subramanian, A. (2020) Investigators, G.-U.-.-. Remdesivir for 5 or 10 Days in Patients with Severe Covid-19. *N. Engl. J. Med. 383* (19), 1827−1837.
(19) Spinner, C. D., Gottlieb, R. L., Criner, G. J., Arribas López, J. R., Cattelan, A. M., Soriano Viladomiu, A., Ogbuagu, O., Malhotra, P., Mullane, K. M., Castagna, A., Chai, L. Y. A., Roestenberg, M., Tsang, O. T. Y., Bernasconi, E., Le Turnier, P., Chang, S. C., SenGupta, D., Hyland, R. H., Osinusi, A. O., Cao, H., Blair, C., Wang, H., Gaggar, A., Brainard, D. M., McPhail, M. J., Bhagani, S., Ahn, M. Y., Sanyal, A. J., Huhn, G., Marty, F. M., and Investigators, G.-U. (2020) Effect of Remdesivir vs Standard Care on Clinical Status at 11 Days in Patients With Moderate COVID-19: A Randomized Clinical Trial. *JAMA 324* (11), 1048−1057.
(20) Sun, D. (2020) Remdesivir for Treatment of COVID-19: Combination of Pulmonary and IV Administration May Offer Aditional Benefit. *AAPS J. 22* (4), 77.
(21) Bouhaddou, M., Memon, D., Meyer, B., White, K. M., Rezelj, V. V., Correa Marrero, M., Polacco, B. J., Melnyk, J. E., Ulferts, S., Kaake, R. M., Batra, J., Richards, A. L., Stevenson, E., Gordon, D. E., Rojc, A., Obernier, K., Fabius, J. M., Soucheray, M., Miorin, L., Moreno, E., Koh, C., Tran, Q. D., Hardy, A., Robinot, R., Vallet, T., Nilsson-Payant, B. E., Hernandez-Armenta, C., Dunham, A., Weigang, S., Knerr, J., Modak, M., Quintero, D., Zhou, Y., Dugourd, A., Valdeolivas, A., Patil, T., Li, Q., Hüttenhain, R., Cakir, M., Muralidharan, M., Kim, M., Jang, G., Tutuncuoglu, B., Hiatt, J., Guo, J. Z., Xu, J., Bouhaddou, S., Mathy, C. J. P., Gaulton, A., Manners, E. J., Félix, E., Shi, Y., Goff, M., Lim, J. K., McBride, T., O'Neal, M. C., Cai, Y., Chang, J. C. J., Broadhurst, D. J., Klippsten, S., De Wit, E., Leach, A. R., Kortemme, T., Shoichet, B., Ott, M., Saez-Rodriguez, J., tenOever, B. R., Mullins, R. D., Fischer, E. R., Kochs, G., Grosse, R., García-Sastre, A., Vignuzzi, M., Johnson, J. R., Shokat, K.

https://doi.org/10.1021/acsinfecdis.1c00017
ACS Infect. Dis. XXXX, XXX, XXX−XXX

M., Swaney, D. L., Beltrao, P., and Krogan, N. J. (2020) The Global Phosphorylation Landscape of SARS-CoV-2 Infection. *Cell 182* (3), 685−712.e19.
(22) Riva, L., Yuan, S., Yin, X., Martin-Sancho, L., Matsunaga, N., Pache, L., Burgstaller-Muehlbacher, S., De Jesus, P. D., Teriete, P., Hull, M. V., Chang, M. W., Chan, J. F., Cao, J., Poon, V. K., Herbert, K. M., Cheng, K., Nguyen, T. H., Rubanov, A., Pu, Y., Nguyen, C., Choi, A., Rathnasinghe, R., Schotsaert, M., Miorin, L., Dejosez, M., Zwaka, T. P., Sit, K. Y., Martinez-Sobrido, L., Liu, W. C., White, K. M., Chapman, M. E., Lendy, E. K., Glynne, R. J., Albrecht, R., Ruppin, E., Mesecar, A. D., Johnson, J. R., Benner, C., Sun, R., Schultz, P. G., Su, A. I., García-Sastre, A., Chatterjee, A. K., Yuen, K. Y., and Chanda, S. K. (2020) Discovery of SARS-CoV-2 antiviral drugs through large-scale compound repurposing. *Nature 586* (7827), 113−119.
(23) Dittmar, M., Lee, J. S., Whig, K., Segrist, E., Li, M., Kamalia, B., Castellana, L., Ayyanathan, K., Cardenas-Diaz, F. L., Morrisey, E. E., Truitt, R., Yang, W., Jurado, K., Samby, K., Ramage, H., Schultz, D. C., and Cherry, S. (2021) Drug repurposing screens reveal cell-type-specific entry pathways and FDA-approved drugs active against SARS-Cov-2. *Cell Rep. 35* (1), 108959.
(24) Hoffmann, M., Hofmann-Winkler, H., Smith, J. C., Krüger, N., Arora, P., Sørensen, L. K., Søgaard, O. S., Hasselstrøm, J. B., Winkler, M., Hempel, T., Raich, L., Olsson, S., Danov, O., Jonigk, D., Yamazoe, T., Yamatsuta, K., Mizuno, H., Ludwig, S., Noé, F., Kjolby, M., Braun, A., Sheltzer, J. M., and Pöhlmann, S. (2021) Camostat mesylate inhibits SARS-CoV-2 activation by TMPRSS2-related proteases and its metabolite GBPA exerts antiviral activity. *EBioMedicine 65*, 103255.
(25) Krump-Konvalinkova, V., Bittinger, F., Unger, R. E., Peters, K., Lehr, H. A., and Kirkpatrick, C. J. (2001) Generation of human pulmonary microvascular endothelial cell lines. *Lab. Invest. 81* (12), 1717−27.
(26) Fu, L., Ye, F., Feng, Y., Yu, F., Wang, Q., Wu, Y., Zhao, C., Sun, H., Huang, B., Niu, P., Song, H., Shi, Y., Li, X., Tan, W., Qi, J., and Gao, G. F. (2020) Both Boceprevir and GC376 efficaciously inhibit SARS-CoV-2 by targeting its main protease. *Nat. Commun. 11* (1), 4417.
(27) Froggatt, H. M., Heaton, B. E., and Heaton, N. S. (2020) Development of a Fluorescence-Based, High-Throughput SARS-CoV-2 3CL. *J. Virol. 94* (22), e01265-20.
(28) Lin, M. H., Moses, D. C., Hsieh, C. H., Cheng, S. C., Chen, Y. H., Sun, C. Y., and Chou, C. Y. (2018) Disulfiram can inhibit MERS and SARS coronavirus papain-like proteases via different modes. *Antiviral Res. 150*, 155−163.
(29) Chen, T., Fei, C.-Y., Chen, Y.-P., Sargsyan, K., Chang, C.-P., Yuan, H. S., and Lim, C. (2021) Synergistic Inhibition of SARS-CoV-2 Replication Using Disulfiram/Ebselen and Remdesivir. *ACS Pharmacology & Translational Science 4* (2), 898−907.
(30) Hu, J. J., Liu, X., Xia, S., Zhang, Z., Zhang, Y., Zhao, J., Ruan, J., Luo, X., Lou, X., Bai, Y., Wang, J., Hollingsworth, L. R., Magupalli, V. G., Zhao, L., Luo, H. R., Kim, J., Lieberman, J., and Wu, H. (2020) FDA-approved disulfiram inhibits pyroptosis by blocking gasdermin D pore formation. *Nat. Immunol. 21* (7), 736−745.
(31) Kitson, T. M. (1975) The effect of disulfiram on the aldehyde dehydrogenases of sheep liver. *Biochem. J. 151* (2), 407−12.
(32) Nguyenla, X., Wehri, E., Van Dis, E., Biering, S. B., Yamashiro, L. H., Stroumza, J., Dugast-Darzacq, C., Graham, T., Stanley, S., and Schaletzky, J. (2020) Discovery of SARS-CoV-2 antiviral synergy between remdesivir and approved drugs in human lung cells. *bioRxiv*, DOI: 10.1101/2020.09.18.302398.
(33) Yadav, B., Wennerberg, K., Aittokallio, T., and Tang, J. (2015) Searching for Drug Synergy in Complex Dose-Response Landscapes Using an Interaction Potency Model. *Comput. Struct. Biotechnol. J. 13*, 504−13.
(34) Hoffmann, M., Kleine-Weber, H., and Pöhlmann, S. (2020) A Multibasic Cleavage Site in the Spike Protein of SARS-CoV-2 Is Essential for Infection of Human Lung Cells. *Mol. Cell 78* (4), 779−784.e5.
(35) Hoffmann, M., Kleine-Weber, H., Schroeder, S., Krüger, N., Herrler, T., Erichsen, S., Schiergens, T. S., Herrler, G., Wu, N. H., Nitsche, A., Müller, M. A., Drosten, C., and Pöhlmann, S. (2020) SARS-CoV-2 Cell Entry Depends on ACE2 and TMPRSS2 and Is Blocked by a Clinically Proven Protease Inhibitor. *Cell 181* (2), 271−280.e8.
(36) Matsuyama, S., Nao, N., Shirato, K., Kawase, M., Saito, S., Takayama, I., Nagata, N., Sekizuka, T., Katoh, H., Kato, F., Sakata, M., Tahara, M., Kutsuna, S., Ohmagari, N., Kuroda, M., Suzuki, T., Kageyama, T., and Takeda, M. (2020) Enhanced isolation of SARS-CoV-2 by TMPRSS2-expressing cells. *Proc. Natl. Acad. Sci. U. S. A. 117* (13), 7001−7003.
(37) Ou, X., Liu, Y., Lei, X., Li, P., Mi, D., Ren, L., Guo, L., Guo, R., Chen, T., Hu, J., Xiang, Z., Mu, Z., Chen, X., Chen, J., Hu, K., Jin, Q., Wang, J., and Qian, Z. (2020) Characterization of spike glycoprotein of SARS-CoV-2 on virus entry and its immune cross-reactivity with SARS-CoV. *Nat. Commun. 11* (1), 1620.
(38) Liu, T., Luo, S., Libby, P., and Shi, G. P. (2020) Cathepsin L-selective inhibitors: A potentially promising treatment for COVID-19 patients. *Pharmacol. Ther. 213*, 107587.
(39) Pruijssers, A. J., George, A. S., Schäfer, A., Leist, S. R., Gralinksi, L. E., Dinnon, K. H., Yount, B. L., Agostini, M. L., Stevens, L. J., Chappell, J. D., Lu, X., Hughes, T. M., Gully, K., Martinez, D. R., Brown, A. J., Graham, R. L., Perry, J. K., Du Pont, V., Pitts, J., Ma, B., Babusis, D., Murakami, E., Feng, J. Y., Bilello, J. P., Porter, D. P., Cihlar, T., Baric, R. S., Denison, M. R., and Sheahan, T. P. (2020) Remdesivir Inhibits SARS-CoV-2 in Human Lung Cells and Chimeric SARS-CoV Expressing the SARS-CoV-2 RNA Polymerase in Mice. *Cell Rep. 32* (3), 107940.
(40) Touret, F., Gilles, M., Barral, K., Nougairède, A., van Helden, J., Decroly, E., de Lamballerie, X., and Coutard, B. (2020) In vitro screening of a FDA approved chemical library reveals potential inhibitors of SARS-CoV-2 replication. *Sci. Rep. 10* (1), 13093.
(41) Ahidjo, B. A., Loe, M. W. C., Ng, Y. L., Mok, C. K., and Chu, J. J. H. (2020) Current Perspective of Antiviral Strategies against COVID-19. *ACS Infect. Dis. 6* (7), 1624−1634.
(42) Bakowski, M. A., Beutler, N., Chen, E., Nguyen, T.-T. H., Kirkpatrick, M. G., Parren, M., Yang, L., Ricketts, J., Gupta, A. K., Hull, M. V., Schultz, P. G., Burton, D. R., Chatterjee, A. K., McNamara, C. W., and Rogers, T. F. (2020) Oral drug repositioning candidates and synergistic remdesivir combinations for the prophylaxis and treatment of COVID-19. *bioRxiv*, DOI: 10.1101/2020.06.16.153403.
(43) Yang, C. W., Peng, T. T., Hsu, H. Y., Lee, Y. Z., Wu, S. H., Lin, W. H., Ke, Y. Y., Hsu, T. A., Yeh, T. K., Huang, W. Z., Lin, J. H., Sytwu, H. K., Chen, C. T., and Lee, S. J. (2020) Repurposing old drugs as antiviral agents for coronaviruses. *Biomed J. 43* (4), 368−374.
(44) Jeon, S., Ko, M., Lee, J., Choi, I., Byun, S. Y., Park, S., Shum, D., and Kim, S. (2020) Identification of Antiviral Drug Candidates against SARS-CoV-2 from FDA-Approved Drugs. *Antimicrob. Agents Chemother. 64* (7), e00819-20.
(45) Ko, M., Jeon, S., Ryu, W.-S., and Kim, S. (2021) Comparative analysis of antiviral efficacy of FDA-approved drugs against SARS-CoV-2 in human lung cells. *J. Med. Virol. 93* (3), 1403−1408.
(46) Wei, J., Alfajaro, M. M., DeWeirdt, P. C., Hanna, R. E., Lu-Culligan, W. J., Cai, W. L., Strine, M. S., Zhang, S. M., Graziano, V. R., Schmitz, C. O., Chen, J. S., Mankowski, M. C., Filler, R. B., Ravindra, N. G., Gasque, V., de Miguel, F. J., Patil, A., Chen, H., Oguntuyo, K. Y., Abriola, L., Surovtseva, Y. V., Orchard, R. C., Lee, B., Lindenbach, B. D., Politi, K., van Dijk, D., Kadoch, C., Simon, M. D., Yan, Q., Doench, J. G., and Wilen, C. B. (2021) Genome-wide CRISPR Screens Reveal Host Factors Critical for SARS-CoV-2 Infection. *Cell 184* (1), 76−91.e13.
(47) Daniloski, Z., Jordan, T. X., Wessels, H. H., Hoagland, D. A., Kasela, S., Legut, M., Maniatis, S., Mimitou, E. P., Lu, L., Geller, E., Danziger, O., Rosenberg, B. R., Phatnani, H., Smibert, P., Lappalainen, T., tenOever, B. R., and Sanjana, N. E. (2021) Identification of Required Host Factors for SARS-CoV-2 Infection in Human Cells. *Cell 184* (1), 92−105.e16.
(48) Wu, C. H., Yeh, S. H., Tsay, Y. G., Shieh, Y. H., Kao, C. L., Chen, Y. S., Wang, S. H., Kuo, T. J., Chen, D. S., and Chen, P. J.

https://doi.org/10.1021/acsinfecdis.1c00017
ACS Infect. Dis. XXXX, XXX, XXX−XXX

(2009) Glycogen synthase kinase-3 regulates the phosphorylation of severe acute respiratory syndrome coronavirus nucleocapsid protein and viral replication. *J. Biol. Chem. 284* (8), 5229−39.
(49) Biering, S. B., Sarnik, S. A., Wang, E., Zengel, J. R., Sathyan, V., Nguyenla, X., Van Dis, E., Catamura, C., Yamashiro, L. H., Begeman, A., Stark, J. C., Shon, D. J., Fox, D. M., Puschnik, A. S., Bertozzi, C. R., Carette, J. E., Stanley, S. A., Harris, E., Konermann, S., and Hsu, P. D. (2021) Genome-wide, bidirectional CRISPR screens identify mucins as critical host factors modulating SARS-CoV-2 infection. *bioRxiv*, DOI: 10.1101/2021.04.22.440848.
(50) Wang, R., Simoneau, C. R., Kulsuptrakul, J., Bouhaddou, M., Travisano, K. A., Hayashi, J. M., Carlson-Stevermer, J., Zengel, J. R., Richards, C. M., Fozouni, P., Oki, J., Rodriguez, L., Joehnk, B., Walcott, K., Holden, K., Sil, A., Carette, J. E., Krogan, N. J., Ott, M., and Puschnik, A. S. (2021) Genetic Screens Identify Host Factors for SARS-CoV-2 and Common Cold Coronaviruses. *Cell 184* (1), 106−119.e14.
(51) Huang, F., Motlekar, N. A., Burgwin, C. M., Napper, A. D., Diamond, S. L., and Mazin, A. V. (2011) Identification of specific inhibitors of human RAD51 recombinase using high-throughput screening. *ACS Chem. Biol. 6* (6), 628−35.
(52) Son, K., Nguyen, T. T. T., Choi, J. W., Pham, L. V., Luong, T. T. D., Lim, Y. S., and Hwang, S. B. (2017) Rad51 Interacts with Nonstructural 3 Protein of Hepatitis C Virus and Regulates Viral Production. *Front. Microbiol. 8*, 1249.
(53) Yin, W., Mao, C., Luan, X., Shen, D. D., Shen, Q., Su, H., Wang, X., Zhou, F., Zhao, W., Gao, M., Chang, S., Xie, Y. C., Tian, G., Jiang, H. W., Tao, S. C., Shen, J., Jiang, Y., Jiang, H., Xu, Y., Zhang, S., Zhang, Y., and Xu, H. E. (2020) Structural basis for inhibition of the RNA-dependent RNA polymerase from SARS-CoV-2 by remdesivir. *Science 368* (6498), 1499−1504.
(54) Zhang, L., and Zhou, R. (2020) Structural Basis of the Potential Binding Mechanism of Remdesivir to SARS-CoV-2 RNA-Dependent RNA Polymerase. *J. Phys. Chem. B 124* (32), 6955−6962.
(55) Li, W., Moore, M. J., Vasilieva, N., Sui, J., Wong, S. K., Berne, M. A., Somasundaran, M., Sullivan, J. L., Luzuriaga, K., Greenough, T. C., Choe, H., and Farzan, M. (2003) Angiotensin-converting enzyme 2 is a functional receptor for the SARS coronavirus. *Nature 426* (6965), 450−4.
(56) Zhang, J. H., Chung, T. D., and Oldenburg, K. R. (1999) A Simple Statistical Parameter for Use in Evaluation and Validation of High Throughput Screening Assays. *J. Biomol. Screening 4* (2), 67−73.
(57) Subramanian, A., Tamayo, P., Mootha, V. K., Mukherjee, S., Ebert, B. L., Gillette, M. A., Paulovich, A., Pomeroy, S. L., Golub, T. R., Lander, E. S., and Mesirov, J. P. (2005) Gene set enrichment analysis: a knowledge-based approach for interpreting genome-wide expression profiles. *Proc. Natl. Acad. Sci. U. S. A. 102* (43), 15545−50.
(58) Mootha, V. K., Lindgren, C. M., Eriksson, K. F., Subramanian, A., Sihag, S., Lehar, J., Puigserver, P., Carlsson, E., Ridderstråle, M., Laurila, E., Houstis, N., Daly, M. J., Patterson, N., Mesirov, J. P., Golub, T. R., Tamayo, P., Spiegelman, B., Lander, E. S., Hirschhorn, J. N., Altshuler, D., and Groop, L. C. (2003) PGC-1alpha-responsive genes involved in oxidative phosphorylation are coordinately downregulated in human diabetes. *Nat. Genet. 34* (3), 267−73.
(59) Wittwer, C. T., Herrmann, M. G., Gundry, C. N., and Elenitoba-Johnson, K. S. (2001) Real-time multiplex PCR assays. *Methods 25* (4), 430−42.
(60) Xue, X., Yang, H., Shen, W., Zhao, Q., Li, J., Yang, K., Chen, C., Jin, Y., Bartlam, M., and Rao, Z. (2007) Production of authentic SARS-CoV M(pro) with enhanced activity: application as a novel tag-cleavage endopeptidase for protein overproduction. *J. Mol. Biol. 366* (3), 965−75.

https://doi.org/10.1021/acsinfecdis.1c00017
ACS Infect. Dis. XXXX, XXX, XXX−XXX